



HAL
open science

Implications of the discovery of AF Lep b. The mass-luminosity relation for planets in the β Pic Moving Group and the L-T transition for young companions and free-floating planets

R. Gratton, M. Bonavita, D. Mesa, A. Zurlo, S. Marino, S. Desidera, V. d'Orazi, E. Rigliaco, V. Squicciarini, P. H. Nogueira

► To cite this version:

R. Gratton, M. Bonavita, D. Mesa, A. Zurlo, S. Marino, et al.. Implications of the discovery of AF Lep b. The mass-luminosity relation for planets in the β Pic Moving Group and the L-T transition for young companions and free-floating planets. *Astronomy & Astrophysics*, 2024, 684, 10.1051/0004-6361/202348012 . insu-04853461

HAL Id: insu-04853461

<https://insu.hal.science/insu-04853461v1>

Submitted on 23 Dec 2024

HAL is a multi-disciplinary open access archive for the deposit and dissemination of scientific research documents, whether they are published or not. The documents may come from teaching and research institutions in France or abroad, or from public or private research centers.





L'archive ouverte pluridisciplinaire **HAL**, est destinée au dépôt et à la diffusion de documents scientifiques de niveau recherche, publiés ou non, émanant des établissements d'enseignement et de recherche français ou étrangers, des laboratoires publics ou privés.



Distributed under a Creative Commons Attribution 4.0 International License

Implications of the discovery of AF Lep b

The mass-luminosity relation for planets in the β Pic Moving Group and the L–T transition for young companions and free-floating planets

R. Gratton¹, M. Bonavita^{1,2}, D. Mesa¹, A. Zurlo^{3,4,5}, S. Marino⁶, S. Desidera¹, V. D’Orazi^{1,7}, E. Rigliaco¹, V. Squicciarini^{1,8}, and P. H. Nogueira^{3,5}

¹ INAF – Osservatorio Astronomico di Padova, Vicolo dell’Osservatorio 5, 35122 Padova, Italy
e-mail: raffaele.gratton@inaf.it

² Institute for Astronomy, University of Edinburgh Royal Observatory, Blackford Hill, EH9 3HJ Edinburgh, UK

³ Instituto de Estudios Astrofísicos, Facultad de Ingeniería y Ciencias, Universidad Diego Portales, Av. Ejército 441, Santiago, Chile

⁴ Escuela de Ingeniería Industrial, Facultad de Ingeniería y Ciencias, Universidad Diego Portales, Av. Ejército 441, Santiago, Chile

⁵ Millennium Nucleus on Young Exoplanets and their Moons (YEMS), Santiago, Chile

⁶ Department of Physics and Astronomy, University of Exeter, Stocker Road, Exeter EX4 4QL, UK

⁷ Dipartimento di Fisica, Università di Roma Tor Vergata, via della Ricerca Scientifica 1, 00133 Roma, Italy

⁸ LESIA, Observatoire de Paris, Université PSL, CNRS, Sorbonne Université, Université Paris Cité, 5 place Jules Janssen, 92195 Meudon, France

Received 18 September 2023 / Accepted 29 January 2024

ABSTRACT

Context. Dynamical masses of young planets aged between 10 and 200 Myr detected in imaging play a crucial role in shaping models of giant planet formation. Regrettably, only a few such objects possess these characteristics. Furthermore, the evolutionary pattern of young sub-stellar companions in near-infrared colour–magnitude diagrams might diverge from free-floating objects, possibly due to differing formation processes.

Aims. The recent identification of a giant planet around AF Lep, part of the β Pic moving group (BPMG), encouraged us to re-examine these points.

Methods. We considered updated dynamical masses and luminosities for the sub-stellar objects in the BPMG. In addition, we compared the properties of sub-stellar companions and free-floating objects in the BPMG and other young associations remapping the positions of the objects in the colour–magnitude diagram into a dustiness–temperature plane.

Results. We found that cold-start evolutionary models do not reproduce the mass-luminosity relation for sub-stellar companions in the BPMG. This aligns rather closely with predictions from “hot start” scenarios and is consistent with recent planet formation models. We obtain rather good agreement with masses from photometry and the remapping approach compared to actual dynamical masses. We also found a strong suggestion that the near-infrared colour–magnitude diagram for young companions is different from that of free-floating objects belonging to the same young associations.

Conclusions. If confirmed by further data, this last result would imply that cloud settling – which likely causes the transition between L and T spectral type – occurs at a lower effective temperature in young companions than in free-floating objects. This might tentatively be explained with a different chemical composition.

Key words. planets and satellites: atmospheres – planets and satellites: formation – planets and satellites: fundamental parameters

1. Introduction

The detection of young planets through direct imaging enables a thorough characterisation of the individual objects. In general, the magnitude and colours can be derived, and in several cases spectra have also been obtained. This allows the derivation of the surface temperature and luminosity, though uncertainties in the model atmospheres make this derivation quite uncertain (see discussion in [Marley & Robinson 2015](#)). The best cases are those of planets at a separation of a few to a few tens of astronomical units that can be detected in stars belonging to very young and nearby associations such as the β Pic Moving Group (BPMG: age of around 20 Myr: [Miret-Roig et al. 2020](#); [Couture et al. 2023](#)). Quite accurate dynamical masses can also be obtained for these objects from their orbit and the motion of the primary,

detected either through space astrometry or high-precision radial velocities ([Samland et al. 2017](#); [Dupuy et al. 2022](#); [Nowak et al. 2020](#); [Franson & Bowler 2023](#)). This is important in order to understand the formation of these objects and to calibrate models that are highly uncertain, especially at young ages. In fact, we expect that the early evolution, and hence the luminosity, of very young planets depends on how they assemble ([Spiegel & Burrows 2012](#)). Namely, a debate exists about the initial entropy of the planets, related to the fact that, in the core-accretion formation scenario of gas giant planets, most of the gas accreting onto a planet is likely processed through an accretion shock ([Marley et al. 2007](#); [Mordasini et al. 2017](#); [Berardo et al. 2017](#)). This shock is key in setting the structure of the forming planet and thus its observable post-formation luminosity. The radiative feedback can change the thermal and chemical structure of the

Table 1. Comparison of parameters for AF Lep b derived in this study with those reported in previous works.

T_{eff} (K)	$\log g$	$\log L/L_{\odot}$	Mass (M_{Jup})	Source	Model
908 ± 123	-3.7 ± 0.3	-4.97 ± 0.20	$3.2^{+0.7}_{-0.6}$	This study	AMES-COND
1000–1700			$5.24^{+0.08}_{-0.10}$	Mesa et al. (2023)	AMES-COND
1030 ± 12	4.00 ± 0.04	-4.75 ± 0.02	$4.3^{+2.9}_{-1.3}$	De Rosa et al. (2023)	AMES-COND, AMES-DUSTY
		-4.81 ± 0.13	$3.2^{+0.7}_{-0.6}$	Franson et al. (2023)	Empirical BC Filippazzo et al. (2015)
789^{+22}_{-20}	3.7	-5.22 ± 0.04	$2.8^{+0.6}_{-0.5}$	Zhang et al. (2023)	petitRadTRANS Mollière et al. (2019)

circum-planetary and local circumstellar disc. Depending on the initial entropy, models with high or low initial luminosities exist (the so-called hot-start and cold-start models), though recent models suggest that hot-start is a better representation of this complex phenomenon (Mordasini et al. 2017; Berardo et al. 2017). A previous analysis based on the planets of β Pic and that of 51 Eri indeed favours a hot start model (Mordasini et al. 2017).

We also recall that several authors (see e.g. Liu et al. 2016; Delorme et al. 2017) have noticed that young sub-stellar objects of L-spectral type appear redder than older ones. This fact is attributed to their lower gravity (see e.g. Baudino et al. 2015), the presence of a higher amount of dust in their atmospheres (Chabrier et al. 2000), or both (Delorme et al. 2017). On the other hand, the luminosity of the L–T transition for free-floating objects seems quite independent of age (Dupuy & Liu 2012; Liu et al. 2016), that is, it occurs at nearly the same effective temperature for objects over a large range of ages. The transition between L and T spectral type (hereinafter L–T transition) is possibly due to the settling of dust in the atmosphere but the details of the process are still not clear (Burrows et al. 2006; Burgasser 2007; Saumon & Marley 2008; Marley et al. 2010; Charnay et al. 2018; Vos et al. 2019), though other scenarios involving the efficiency of vertical mixing in the atmospheres have been proposed (Tremblin et al. 2016). For instance, the models by Charnay et al. (2018) predict that the luminosity of the L–T transition is very sensitive to gravity, suggesting that it should also be sensitive to age, a fact that does not agree with observational data at least for ages < 200 Myr. On the other hand, the size of grains likely matters; larger particles more rapidly ‘rain out’ of the atmosphere, leading to a sudden clearing or collapse of the clouds (Knapp et al. 2004). Finally, the observed J -band brightening across the transition could arise from decreasing cloud coverage (Ackerman & Marley 2001). We notice that while gravity does not separate objects that formed in the disc around stars from free-floating objects that formed in isolation, the presence of different amounts of dust or differences in their size or distribution might depend on their composition and then on the specific formation history of the objects. It would then be important to compare the photometric properties of young planets with those of free-floating objects of similar luminosity and age, searching for any systematic difference. Liu et al. (2016) proposed that there may indeed be some difference, but data for few planets were available at the epoch.

Unfortunately, there are only very few planets with adequate data that have been discovered so far. The addition of a single new case may have significant influence in confirming/rejecting scenarios and models. The recent discovery of a planet around AF Lep (Mesa et al. 2023; De Rosa et al. 2023; Franson et al. 2023), a star belonging to the BPMG, prompted us to review

these crucial aspects of planetary science. Even more recently, Zhang et al. (2023) presented a careful examination of the implications of the spectral energy distribution for AF Lep obtained from the previous studies on the structure of the atmosphere of this planet. This leads to a reliable determination of the effective temperature of the planet and to a strong indication that its atmosphere is much more metal-rich than that of the star.

In this paper, we examine the implications of the discovery of AF Lep b in the derivation of the mass-luminosity relation for planets in the β Pic moving group and on the comparison between the properties of sub-stellar objects that are either star companions or free floating. This paper is organised as follows. In Sect. 2, we present the main parameters for AF Lep b. In Sect. 3, we combine the AF Lep b parameters with those of other members of the BPMG to discuss the mass-luminosity relation for 20 Myr old planets. In Sect. 4, we compare the colour–magnitude diagram for young planets and free-floating objects for the members of the BPMG and of other young associations. We draw conclusions in Sect. 5. The Appendices contain a compilation of data for sub-stellar companions and free-floating objects belonging to young and intermediate age associations used in this paper, and the derivation of a uniform set of temperature and masses for them.

2. Parameters for AF Lep b

Table 1 summarises the parameters for AF Lep b obtained in various papers. We should note that these parameters are not entirely consistent. For instance, the mass and gravity listed by De Rosa et al. (2023) produce a radius of $1.06 R_{\text{Jupiter}}$, which is slightly lower than expected for the mass and age of the planet. Zhang et al. (2023) examined possible inconsistencies in the model atmospheres and their implications. While their analysis for this object is very thorough, we re-derived some of the relevant quantities in order to be consistent with that for the other sub-stellar companions in the BPMG. In our analysis, luminosities $\log L/L_{\odot}$ are obtained from the K -band absolute magnitudes using the bolometric corrections for young ultra-cool dwarfs by Filippazzo et al. (2015). Radii R are obtained by comparison with the AMES COND evolutionary tracks (Baraffe et al. 1998) for an age of 20 Myr. Temperatures are consistent with these values. Errors are obtained by propagating the photometric uncertainties. The effective temperature and luminosity obtained in our analysis of AF Lep are consistent within the errors with those of Zhang et al. (2023), but we notice that we may slightly overestimate the temperature and luminosity of AF Lep b.

We adopted the dynamical mass obtained by Franson et al. (2023) that used a more extensive data set than those considered

Table 2. Parameters for sub-stellar companions in the BPMG.

HIP	Others	Comp	$\log L/L_{\odot}$	M (M_{Jup})	Ref
21547	51 Eri	b	-5.43 ± 0.08	$5.5^{+1.8}_{-3.8}$	Samland et al. (2017); Dupuy et al. (2022)
25486	AF Lep	b	-4.97 ± 0.20	$3.2^{+0.7}_{-0.6}$	Franson et al. (2023)
27321	β Pic	b	-3.80 ± 0.05	11.9 ± 3.0	Nowak et al. (2020)
		c	-4.46 ± 0.07	8.9 ± 0.8	Nowak et al. (2020)
92680	PZ Tel	B	-2.63 ± 0.07	27^{+25}_{-9}	Franson & Bowler (2023)

Notes. Luminosities $\log L/L_{\odot}$ are obtained from the K -band absolute magnitudes using the bolometric corrections by Filippazzo et al. (2015). Errors are obtained by propagating the photometric uncertainties.

by Mesa et al. (2023) and De Rosa et al. (2023). This extensive data set was also considered by Zhang et al. (2023), who, however, derived a slightly lower mass, albeit within the error bars. This is due to the adoption by Zhang et al. (2023) of a lower mass for the primary star, which in turn is a reflection of the sub-solar metal abundance obtained in their analysis. However, this last analysis may be questionable. In fact, it is well known that the metal abundance of young stars is often underestimated due to the impact of their strong activity on the structure of the atmospheres (Baratella et al. 2020). Analyses that take this into account generally produced solar-like values. We think that these small inconsistencies may be attributed to the uncertainties still existing both in data and in models and are reasonably represented by the error bars adopted in this paper.

For completeness, in Table 1 we also give the value of the gravity that can be obtained combining the luminosity, radii, and masses obtained this way. We notice that these parameters are consistent within the errors with those of Zhang et al. (2023).

3. Comparison between dynamical and evolutionary masses

We can use existing data of the dynamical masses of the sub-stellar companions to derive a mass-luminosity relation for the sub-stellar objects in the BPMG. We note here that the age of the BPMG is close to 20 Myr; age estimates (Barrado y Navascués et al. 1999; Mamajek & Bell 2014; Binks & Jeffries 2014; Miret-Roig et al. 2020; Couture et al. 2023) that used a variety of methods range from 18.5 to 22 Myr. Since they are not directly available, luminosities $\log L/L_{\odot}$ were obtained from the K -band absolute magnitudes using the empirical bolometric corrections by Filippazzo et al. (2015). We give the relevant data in Table 2. We compare the observed mass-luminosity relation with the expectations of hot- and cold-start models by Marley et al. (2007; see Fig. 1). We remind the reader that we may overestimate the luminosity of AF Lep b, though at the limit of the error bar. This comparison clearly shows that hot-start models match the observational points much better. Figure 2 compares the observational data with the predictions of the theoretical core accretion models by Mordasini et al. (2017). These models actually predict a range of possible values, depending on the exact history of every single planet; so rather than a single mass-luminosity relation, an intrinsic scatter of the luminosities is expected at each mass and age. In the figure, this is represented by the shaded area between the dashed lines. The comparison between models and observations is reasonably good, in view of the large uncertainties in individual points.

The models by Baraffe et al. (1998) that use the AMES line list are popularly used to derive evolutionary masses for targets

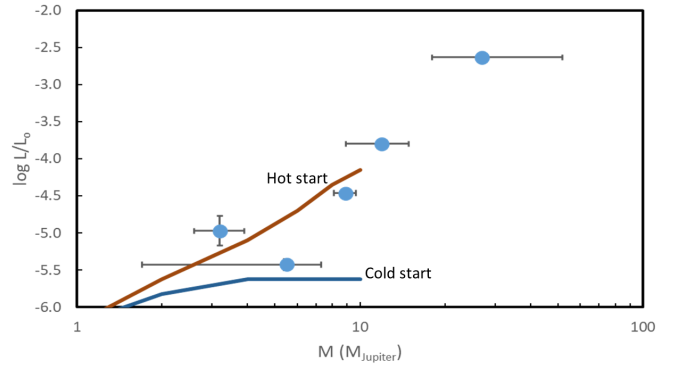


Fig. 1. Dynamical mass–luminosity relation for sub-stellar objects detected in the BPMG compared with the predictions of hot- (brown line) and cold-start (blue line) models by Marley et al. (2007) for an age of 20 Myr.

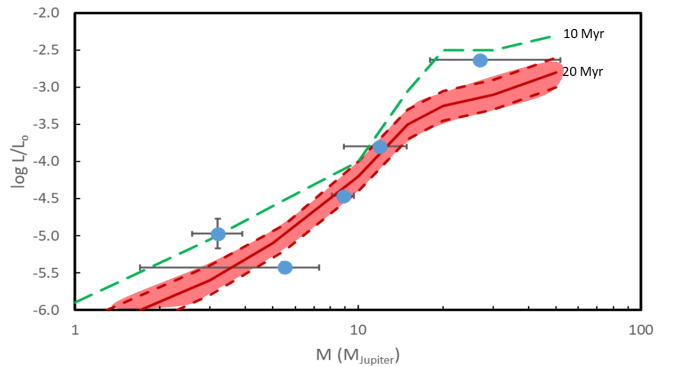


Fig. 2. Dynamical mass–luminosity relation for sub-stellar objects detected in the BPMG. The solid red and the dashed green lines are averages of the predictions by models of Mordasini et al. (2017) for ages of 20 and 10 Myr, respectively. The shaded red region between the dotted red lines represents the range of values that are expected for a 20 Myr age, depending on the peculiar evolution of individual objects.

lacking a dynamical mass. We then show in Fig. 3 the comparison between dynamical masses and those that are derived from the application of these evolutionary models. We show data obtained both with cloudy (AMES-DUSTY; Chabrier et al. 2000) and clear (AMES-COND; Allard et al. 2001) model atmospheres, when using the K magnitude. With the addition of AF Lep b, this is now possible for a total of five companions in the BPMG, the others being the two planets of β Pic, that of 51 Eri, and the brown dwarf (BD) PZ Tel B. For the time being, both models (that correspond to “hot-start” models) pass this test.

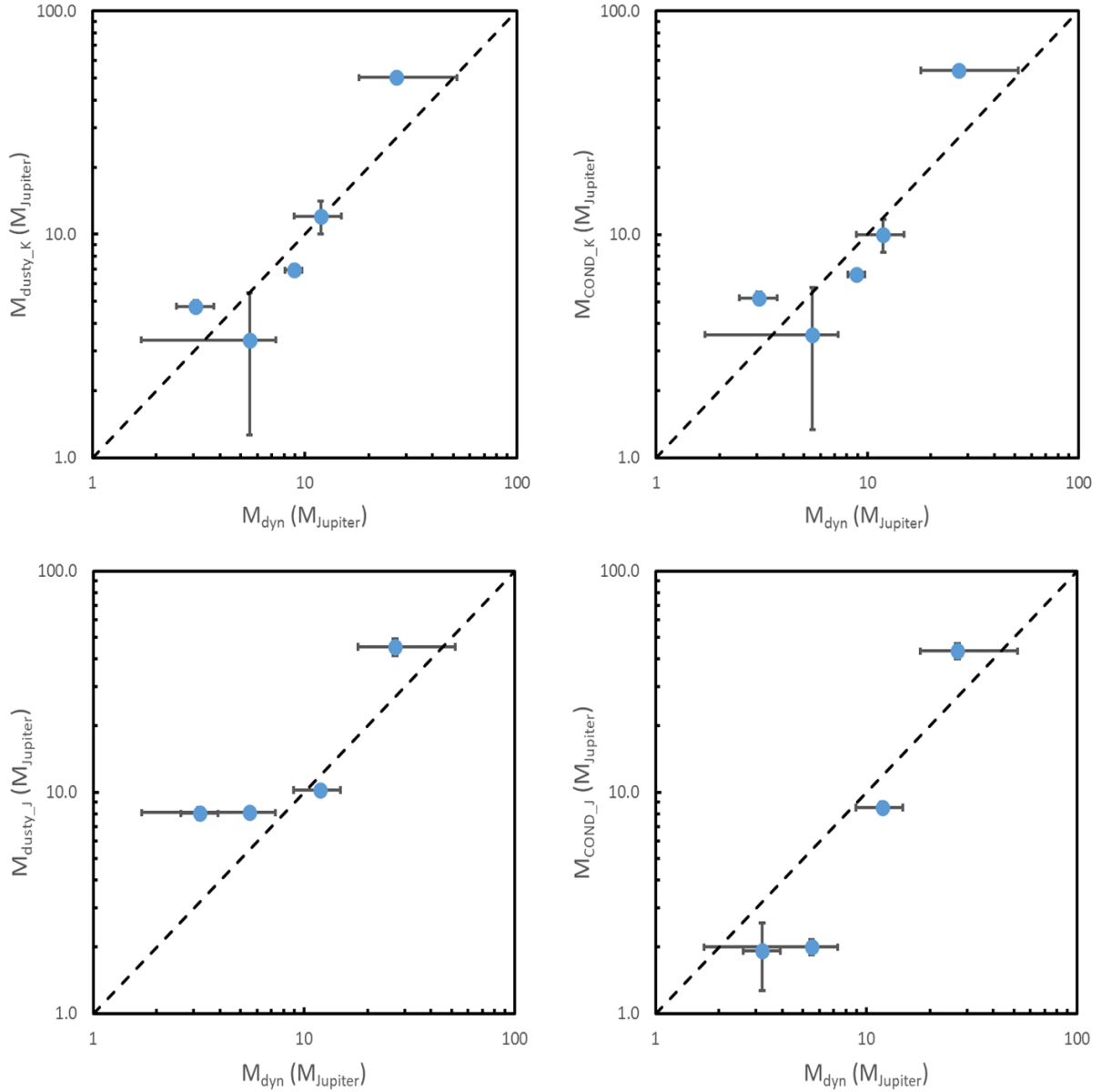


Fig. 3. Comparison between masses obtained from dynamics and those estimated from evolutionary models for the sub-stellar objects detected in the BPMG using the K magnitude (upper row) and the J magnitude (lower row). The left panels are for masses obtained from photometry using the AMES-DUSTY evolutionary models; the right ones are for masses obtained using the AMES-COND evolutionary models. The dashed lines are for equality.

However, both sets of isochrones perform poorly when using the J magnitudes. For this band, the DUSTY models overestimate the masses while the COND ones underestimate them. We empirically found that an average of the two values reproduces the dynamical masses well. This result implies that the models give a poor representation of the $J - K$ colour of the planets. We discuss this point in Sect. 4.

4. Colour-magnitude diagram for young planets and free-floating objects

4.1. Observational data

The location of sub-stellar objects in the BPMG in the colour-magnitude diagram provides further insights into their properties. To give more statistical weight to our results, we

considered both sub-stellar companions and free-floating objects belonging to a number of young populations, in addition to the BPMG: Sco-Cen, Columba, Carina, Argus, Tucana-Horologium, Taurus, Chamaleon, TWA, AB Doradus, and Carina Near. For each of the objects, we checked membership to the respective groups considering the parallaxes, proper motion, and, when available, radial velocities, and using the online BANYAN Σ code (Gagné et al. 2018b)¹. References for the data of the individual objects can be found in Appendix A. In addition, we considered data for sub-stellar objects in the Upper Scorpius association from Lodiéu et al. (2006) and Bouy et al. (2022).

Interpretation of this photometry requires an estimate of the age of the individual objects. In Tables 3 and 4, we report a

¹ <https://www.exoplanetes.umontreal.ca/banyan/banyansigma.php>

Table 3. Ages for associations and moving groups (in Myr).

Reference	BPMG	Columba	Carina	Tuc-Hor	Argus	AB Doradus
Isochrones						
Bell et al. (2015)	24	42	45	45	58	149
Booth et al. (2021)			13			
Lithium						
Barrado y Navascués et al. (2004)					50	
Mentuch et al. (2008)	21			27		>45
Binks & Jeffries (2014)	21					
Malo et al. (2014)	26					
Shkolnik et al. (2017)	22					
Schneider et al. (2019)	22		22			
Wood & Mann (2023)			40			
Kinematics						
McCarthy & Wilhelm (2014)						125
Miret-Roig et al. (2020)	13	>40	>28	>28	37	
Miret-Roig et al. (2020)	19					
Booth et al. (2021)			20			
Kerr et al. (2022)		26	26	46		
Couture et al. (2023)	20					
Mean	21	36	28	37	48	137
Standard deviation	4	8	11	11	10	17

Table 4. Ages for additional associations and moving groups (in Myr).

Associations	Age	Reference
Taurus	1–2	
Chamaleon	1–2	
ϵ Cha	11	Bell et al. (2015)
TWA	10	Bell et al. (2015)
Upper Scorpius	8–12	Pecaut & Mamajek (2016)
Upper Centaurus-Lupus	12–16	Pecaut & Mamajek (2016)
Lower Centaurus-Crux	16	Pecaut & Mamajek (2016)
Carina Near	200	Zuckerman et al. (2006)

number of literature determination of ages for the various associations and moving groups considered in this paper. The values we adopted are the straight averages. In this work, we did not consider the ages by Ujjwal et al. (2020) because they are much lower than and uncorrelated with other estimates. In addition, Gagné et al. (2018a) reported an age of 117 ± 26 Myr for the AB Dor using the massive white dwarf GD 50. While we did not use this estimate here, it is consistent within the errors with the value we adopted.

We show the $(M_K, J - K)$ and the $(M_K, H - K)$ colour magnitude diagrams for these objects in Figs. 4 and 5, respectively. These figures show that the most massive sub-stellar companions of the BPMG (those with $M_K < 12.5$) are indistinguishable in this diagram from the free-floating objects and from members of the other associations of different ages if they are older than 10–15 Myr. This agrees with earlier findings that the colour-magnitude diagram of sub-stellar objects does not change much for ages less than a few hundred million years (Faherty et al. 2016). However, the case is different for fainter objects. While

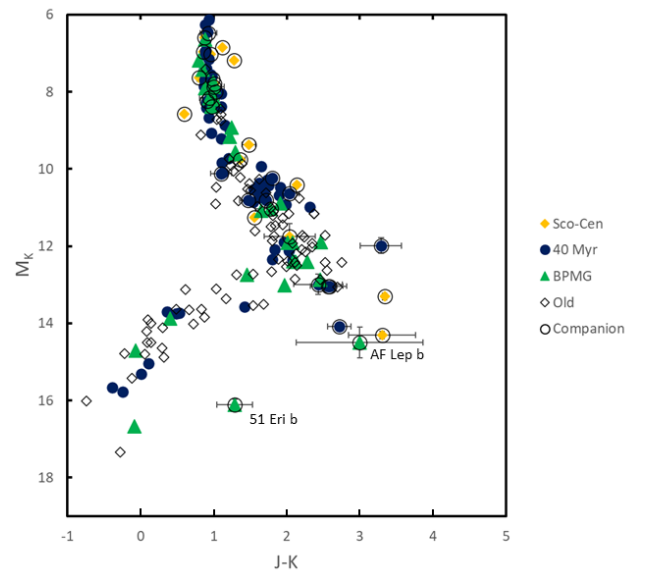


Fig. 4. $(M_K - J - K)$ colour-magnitude diagram for sub-stellar objects in BPMG (green-filled triangles). Sub-stellar object members of Sco-Cen (orange diamonds), young nearby associations with ages in the range of 40–50 Myr (blue-filled circles), and older ones (open blue diamonds) are also plotted. Blue circles mark objects that are companions of more massive objects.

the L–T transition² occurs at magnitudes in the range $M_K \sim 13$ for free-floating objects (irrespective of their age, at least in this

² We do not actually use spectral types throughout this paper; we use the term L–T transition because it is the appearance of very strong molecular bands – faint in L-type spectra and prominent in T-type ones which causes the change in $J - K$ colour from very red to blue.

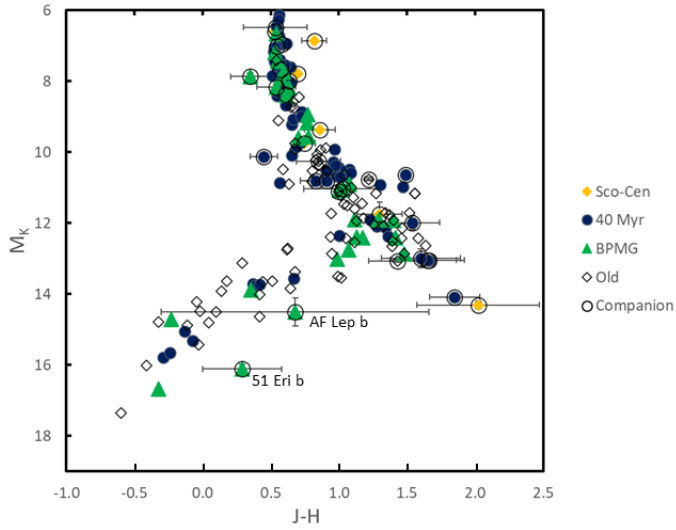


Fig. 5. ($M_K, J - H$) colour–magnitude diagram for sub-stellar objects in the BPMG (green filled triangles). Sub-stellar objects members of the Sco-Cen (orange diamonds), of young nearby associations with ages in the range of 40–50 Myr (blue-filled circles) and of older ones (empty blue diamonds) are also plotted. Blue circles mark objects that are companions of more massive objects.

range), fainter companions are still on the L-sequence down to $M_K \sim 14.5$. There are in fact five planets with $13.3 < M_K < 15$ and $J - K > 2.5$; they are AF Lep b, HR8799b, HD95086b, TYC 8998-760-1c, PDS-70c. Admittedly, PDS-70c may be reddened by the circumstellar (projected towards the planet) and/or circumplanetary disc, so we preferred not to consider it. Still, there are at least four extremely red planets that have no counterpart among the free-floating objects. On the other hand, there is no known planetary companion with $J - K < 1.5$ and $13.3 < M_K < 15$, which is a region populated by more than 20 young free-floating objects. Again, this is not very sensitive to age; in fact, the same occurs for companions in the other associations considered in the plot.

We must caution that this might in part be due to some selection effect. Indeed, detection of such faint and red objects is very difficult and they may have been missed in the surveys looking for low-mass free-floating objects in these young associations. For instance, very recently [Schneider et al. \(2023\)](#) announced the discovery of an extremely red free-floating object in the BPMG (WISE J050626.96+073842.4) with $M_K = 12.99$ and $J - K = 2.97$. In the ($M_K, J - K$) colour–magnitude diagram, this object occupies a position very similar to those of the inner planets of HR8799, but it still is brighter than the four planets considered above. In addition, we notice that free-floating objects with a mass of 5–6 M_{Jup} in the BPMG such as 2MASS J08195820-0335266 and CFBDS J232304-015232³ have a late-T spectral type and a bright M_K magnitude of around 14 ([Zhang et al. 2021](#)). These objects are roughly as massive as 51 Eri b and AF Lep b, which are a factor of ten fainter in the J band. The comparison with slightly older objects in other associations suggests that these two free-floating T-objects are not exceptional. [Liu et al. \(2016\)](#) already noticed the existence of systematic differences

³ The masses for these two objects are $6.16 \pm 0.55 M_{\text{Jup}}$ and $5.13 \pm 0.44 M_{\text{Jup}}$, using the approach described later in this section.

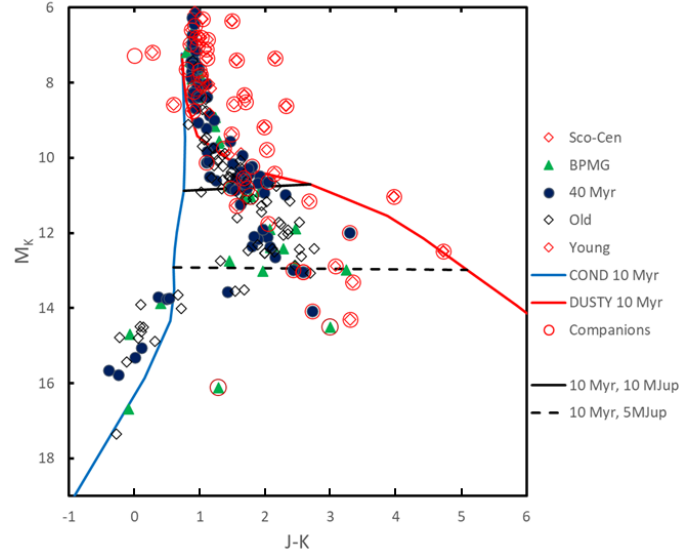


Fig. 6. Same as Fig. 4, but with the inclusion of associations younger than 10 Myr (red circles). Red circles mark objects that are companions of more massive objects. Solid blue and red lines are the predictions of AMES-COND and AMES-DUSTY isochrones with an age of 10 Myr. The solid and dashed black lines connect the points corresponding to the COND and DUSTY AMES isochrones for an age of 10 Myr and masses of 10 and 5 M_{Jup} , respectively. These nearly horizontal iso-mass lines shown here are representative of other masses and ages that span the relevant range of the analysis.

between the colour–magnitude diagram of young free-floating and companion sub-stellar objects.

4.2. Remapping data in a temperature – relevance of dust plane

We remind the reader that while alternative scenarios have been proposed (see [Tremblin et al. 2016](#)), the L–T transition is attributed by most authors to the settling of clouds in the atmospheres that are thought to be very abundant in L-type objects. This is shown by a comparison of the observed location of stars in the ($M_K, J - K$) colour–magnitude diagram with AMES-COND and DUSTY isochrones (see Fig. 6). As mentioned previously, these isochrones use the same evolutionary tracks (that assume a hot start) but different model atmospheres. By definition, the COND atmospheres have no clouds. On the other hand, DUSTY atmospheres are very rich in dust because they assume no settling – while some dust sedimentation is generally expected ([Marley et al. 2010](#); [Morley et al. 2012](#)). While the L-sequence is close to the AMES DUSTY isochrone, the late T sequence is close to the AMES-COND one. For free-floating objects, the L–T transition occurs at an absolute K magnitude between 13 and 14, which, for the age of the BPMG corresponds to a mass of about 5 M_{Jup} . An extension of the survey to older associations (AB Doradus and Carina-Near) shows that the magnitude at which the L–T transition occurs is rather stable over a quite wide range of ages ([Liu et al. 2016](#); see also Fig. 6).

To show the relation between the effective temperature and the transition from cloudy to clean atmospheres, we remapped the colour–magnitude diagram (cmd) into an effective temperature – relevance of dust plane. In our approach, this last effect is represented by a parameter r . To obtain this parameter, we started from the AMES-COND and AMES-DUSTY isochrones. As

mentioned earlier, these isochrones correspond to the same internal model (hence, the same age, mass, temperature, and luminosity), but they use different model atmospheres that project into very different sequences in the near infrared (NIR) cmds. For a given age, for any value of T_{eff} (or mass) we may then define two points in the cmd corresponding to the COND and DUSTY isochrones. By linear interpolation between these points, we can define a new isochrone that corresponds to any arbitrary value of r , where $r = 0$ for the AMES-COND isochrones and $r = 1$ for the AMES-DUSTY one. Hence, a higher value of r qualitatively corresponds to higher dust relevance in the atmosphere. Since the AMES-COND and AMES-DUSTY models are not perfect, very dusty or clean atmospheres do not actually correspond to $r = 1$ or 0. In particular, while the AMES-COND models are quite good representations of a clean atmosphere in this context, the dust-rich atmospheres are much less red than expected from AMES-DUSTY models and correspond to a value of $r \sim 0.5$ rather than $r \sim 1$. However, the relative scale is still valid, at least for $T_{\text{eff}} < 1800$ K. At high temperatures, colour predictions with AMES-COND and AMES-DUSTY models are quite similar, and the value of r becomes uncertain. This result has a weak dependence on age that acts on the radius and then on the magnitude, and it should thus be taken into account. Through this remapping, the location in the NIR cmd for each object (its absolute magnitude and colour) corresponds to a pair of values of T_{eff} and r .

In practice, we ran a Monte Carlo procedure for each star extracting 100 random values of age from a Gaussian distribution with the appropriate mean values and standard deviations. For each of these random sets of ages, we also extracted values of colour and magnitude again with Gaussian distributions with means equal to the best value and standard deviations equal to the error appropriate to the observation of star. For each run of the Monte Carlo procedure, we then constructed maps of colour and magnitude as a function of mass and value of r with a very fine grid in both quantities. We then found where the quadratic sum of the differences between the predicted colour and absolute magnitude and the 'observed' values given by the Monte Carlo procedure described above are minimised. The final best values of mass and r are the mean of the values obtained this way, and the error is the standard deviation of these values. When constructing the maps, we considered values of r in the range of $-0.8 \div 1.9$; values outside the range $0 \div 1$ were obtained by simple linear extrapolation of those corresponding to COND and DUSTY isochrones.

We considered this procedure for both the $(M_K, (J - H))$ and $(M_K, (J - K))$ cmds and we called the two values of r obtained for each diagram $r(J - H)$ and $r(J - K)$. We also obtained a value that we called $r(\text{mean})$, which is the weighted average of the two values.

Figure 7 compares the effective temperatures obtained using this approach with T_{eff} obtained from luminosities derived from the K -band magnitudes and bolometric corrections from [Filippazzo et al. \(2015\)](#), combined with evolutionary radii for young objects. In addition, we repeated the same analysis for the objects listed by [Dupuy & Liu \(2017\)](#); see Fig. 8). The brown dwarf binaries considered in this last paper are mainly old ones (age > 271 Myr). Moreover, all T_{eff} values by [Dupuy & Liu \(2017\)](#) are > 1000 K, and among those with ages < 1 Gyr, the coolest one is Gl 417C with $T_{\text{eff}} = 1560$ K. In both cases, there is an excellent agreement for the stars cooler than 1800 K, while our procedure gives large errors for higher T_{eff} values. This is because at $T_{\text{eff}} > 1800$ K DUSTY and COND isochrones are

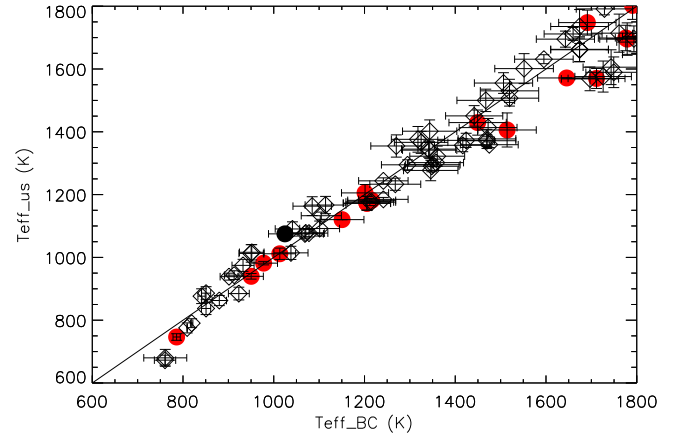


Fig. 7. Comparison between T_{eff} obtained from luminosities derived from K -band magnitudes and bolometric corrections from [Filippazzo et al. \(2015\)](#), combined with evolutionary radii, with the T_{eff} obtained from our remapping approach. Filled red circles represent companions within 1000 au, filled black circles represent companions outside 1000 au, and open diamonds represent free-floating objects or very wide companions (separation > 1000 au). The solid line represents equality.

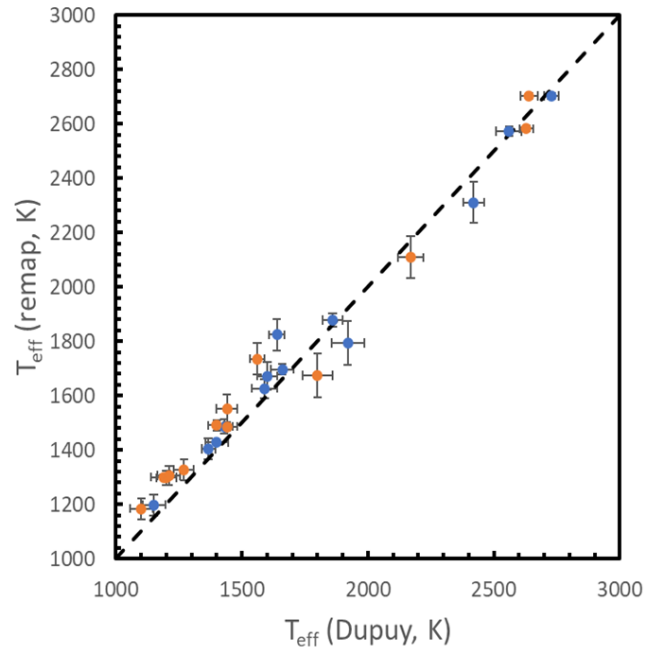


Fig. 8. Comparison between T_{eff} values obtained by [Dupuy & Liu \(2017\)](#) with those obtained from our remapping approach for their sample of BD binaries. Blue symbols are primaries, orange ones are secondaries.

essentially coincident, and the value of the dustiness parameter r has large errors.

We derived internal errors on the T_{eff} from the remapping procedure considering photometric errors and comparing results from $J - H$ and $J - K$. We obtained a mean quadratic value of ± 34 K for stars with $T_{\text{eff}} < 1800$ K, while errors are as high as ± 175 K for stars warmer than this limit. Since both these results depend on the J magnitude, they are not independent of each other. Hence, tests with temperatures obtained using different methods, e.g. from the K -magnitudes, bolometric corrections, and radii from models, are more meaningful. We compared

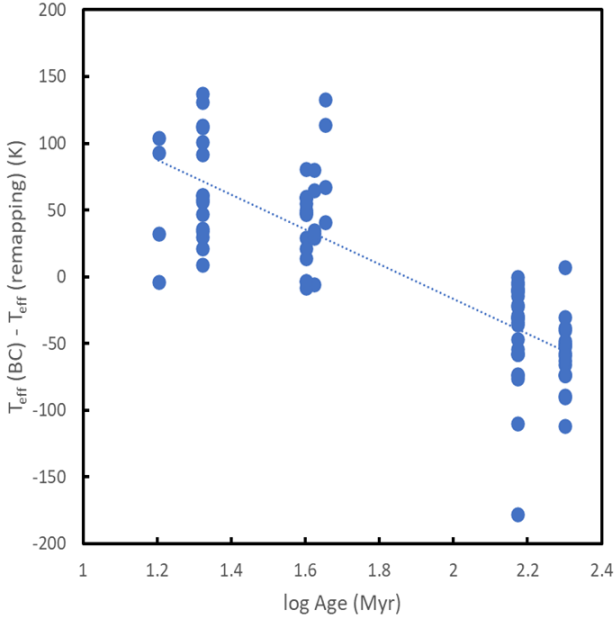


Fig. 9. Run of offset between T_{eff} from BC and remapping as a function of the age for sub-stellar objects with $T_{\text{eff}} < 1800$ K. The dashed line corresponds to Eq. (1) in the text.

the T_{eff} obtained from remapping with those obtained from bolometric magnitudes. If we limit ourselves to objects with $T_{\text{eff}} < 1800$ K, temperatures obtained by remapping are, on average, lower by 9 ± 7 K, with an rms of the difference of 65 K. This corresponds fairly well to the internal errors of 47 and 34 K obtained for the temperatures from bolometric magnitudes and remapping, respectively. We notice that for stars cooler than 1800 K, the residuals are a clear function of age (see Fig. 9), and they are represented by the following relation⁴:

$$T_{\text{eff remapping}} - T_{\text{eff BC}} = 130.35 \log(\text{Age/Myr}) - 244 \text{ K} \quad (1)$$

Root mean square residuals around this relation are only ± 37 K, which is consistent with the internal errors of each of the two relations. This fact can be attributed to our use of a unique BC relation (the one appropriate to young BDs) from Filippazzo et al. (2015), while the same authors acknowledge that this should depend on age. This suggests that in this temperature range, the two methods provide nearly equally accurate T_{eff} values.

We also compared the T_{eff} obtained by our approach with those obtained by Dupuy & Liu (2017), which also used K magnitudes, bolometric corrections, and radii from models. Most of the stars they considered are warmer than 1800 K. On average our T_{eff} are higher by 37 ± 17 K; residuals have an rms of 86 K. Considering that the internal error of Dupuy & Liu (2017) is 40 K, we may estimate that our T_{eff} for these stars have errors of 75 K.

Figure 10 shows the run of the $J - K$ colour as a function of the T_{eff} obtained from the K magnitude, the bolometric corrections by Filippazzo et al. (2015) and radii from evolutionary models. This figure (that is actually very similar to the colour-magnitude diagram shown in Fig. 5 save for the inversion of the

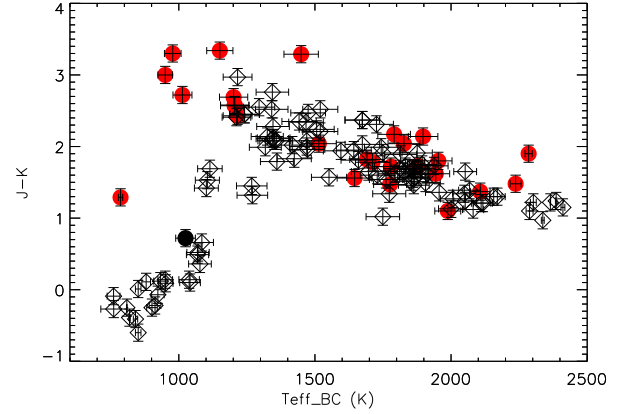


Fig. 10. Run of $J - K$ colour as a function of T_{eff} obtained from K magnitude, bolometric corrections by Filippazzo et al. (2015) and radii from evolutionary models. Filled red circles are companions within 1000 au, filled black circles show companions outside 1000 au, and open diamonds show free floating objects or very wide companions (separation > 1000 au).

axes) shows the expected difference between planets and free-floating objects, with the group of cool and very red planets at $T_{\text{eff}} < 1100$ K and $J - K \sim 3$, a region where there is no free-floating object. For better insight into the nature of this difference, Fig. 11 shows the results of our remapping into the $T_{\text{eff}} - r$ plane for the sub-stellar objects with ages in the range of 10–200 Myr listed in the appendix. Different symbols are used for companions and free-floating objects. As can be seen, as soon as the temperature of a free-floating sub-stellar object falls below ~ 1200 K (this is indeed the direction of the evolution of these objects) the r parameter drops, indicating that clouds settle and the atmosphere becomes quite transparent. However, companions (at least those with separation < 1000 au) behave differently, and cloud settling occurs at a much lower temperature (< 1000 K). This results in the existence of extremely red objects with $M_J > 16.5$ and $J - K > 2.7$, such as HR8799b, HD 95086b, and TYC 8998-760-1c, that have no counterparts among free-floating objects. In addition, the atmosphere of AF Lep b, with $T_{\text{eff}} = 789^{+22}_{-20}$ K, still looks very dust-rich (a fact already noticed by Zhang et al. 2023). 51 Eri b is also redder than free-floating objects with the same temperature.

A secondary but interesting output of the remapping of the sub-stellar objects in the $T_{\text{eff}} - r$ plane is the possibility of obtaining a homogeneous set of evolutionary masses for them. This is given in Table B.1. These masses can be compared with the dynamical masses for the planets in the BPMG as well as for those around HR 8799 in the Columba association (Zurlo et al. 2022; see Fig. 12). The agreement is good. We also compared the masses with those of Dupuy & Liu (2017) and again found good agreement. On average our masses are lower by $-2.6 \pm 1.4 M_{\text{Jup}}$, which is less than 5%; residuals have an r.m.s. of $7.3 M_{\text{Jup}}$, which agrees fairly well with the combinations of the internal errors of Dupuy & Liu (2017; $6.5 M_{\text{Jup}}$) and from our formulas ($1.8 M_{\text{Jup}}$). However, we notice that our approach requires independent knowledge of the ages. Unluckily, this is not the case for the binaries considered by Dupuy & Liu (2017). The age they gave for a number of their targets is actually derived from fitting models to their observational data (magnitudes and dynamical masses). It is then not surprising that we found extremely good agreement between the masses that we may obtain from photometry and their dynamical masses. For these stars, the result only

⁴ The age distribution of the sub-stellar objects considered in this paper actually consist of two groups: young objects with ages < 50 Myr and older ones with ages > 140 Myr. This fact is responsible for the apparent presence of two separate sequences in Fig. 7.

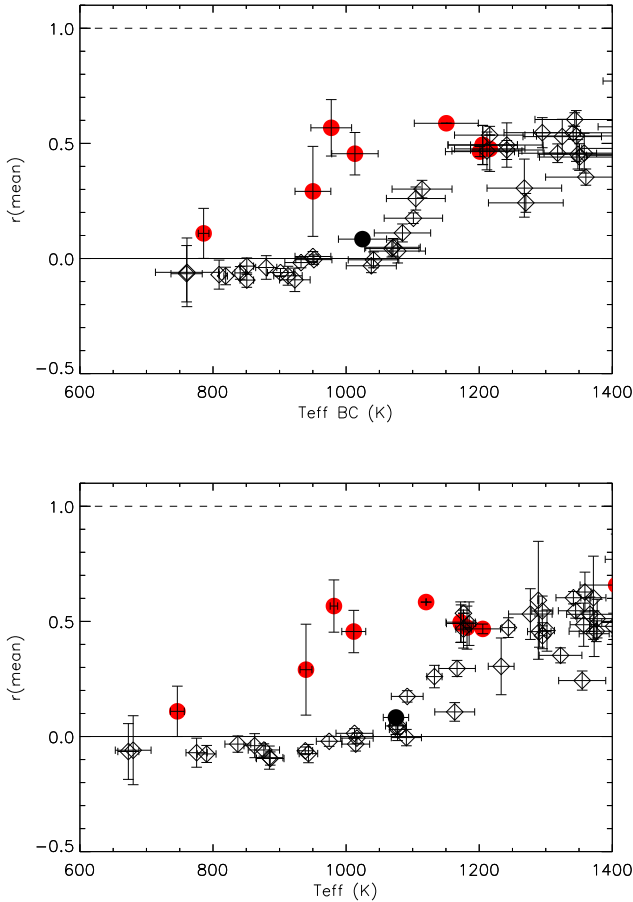


Fig. 11. Remapping of positions of stars from colour–magnitude diagram (cmd) into plan T_{eff} versus dust relevance parameter r (see text) for sub-stellar objects with ages in the range 10–200 Myr. The upper panel shows results obtained using T_{eff} obtained from luminosities derived from the K band magnitudes and bolometric corrections from Filippazzo et al. (2015), combined with evolutionary radii. The lower panel shows T_{eff} from our remapping approach. In both panels, filled red circles are companions within 1000 au, filled black circles show companions outside 1000 au, and open diamonds show free-floating objects or very wide companions (separation >1000 au). The solid and dashed lines represent the expectations for AMES-COND and AMES-DUSTY models, respectively.

shows that the two analyses are consistent with each other, but not that the photometric masses are correct.

4.3. Why the L–T transition for companions occurs at a different temperature from that of free-floating objects

While the statistics is still limited, the results of this section suggest that temperature and gravity (and then age) are not the only parameters controlling cloud settling. Given the complexity of cloud physics, there are various possible explanations. For instance, the models by Charnay et al. (2018) show that the difference between companions (such as AF Lep b) and free-floating objects of similar mass and age (such as 2MASS J08195820-0335266 and CFBDS J232304-015232) might be obtained if the size of dust grains in the atmospheres of companions is smaller than that in the atmospheres of free-floating objects. Such a difference might perhaps be related to a systematic difference in the chemical composition. Early analysis concluded that young planets that accrete gas from the disc will most likely have a strongly

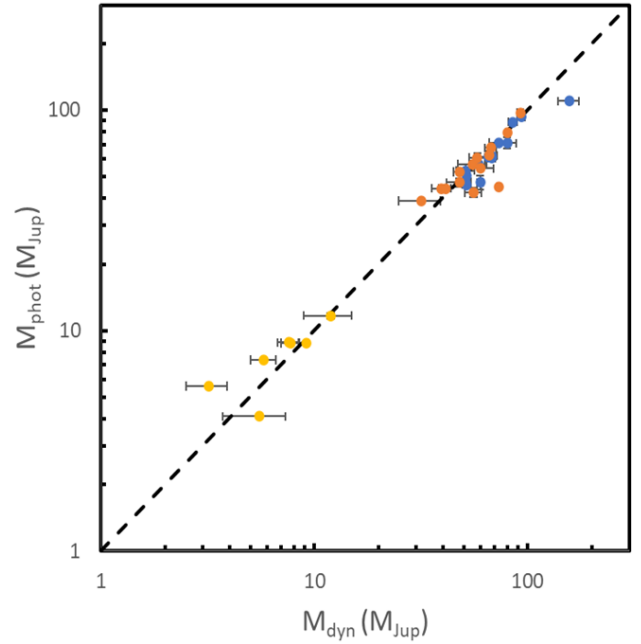


Fig. 12. Comparison between masses obtained from dynamics and those estimated from evolutionary models for sub-stellar objects. Evolutionary masses were obtained from the AMES isochrones using the approach described in this paper. Yellow symbols represent planetary companions; blue-filled circles show primaries and orange symbols show secondaries from the binary BD sample of Dupuy & Liu (2017). The dashed line is for equality.

oxygen-depleted atmosphere (Helling et al. 2014). The grain seed formation rate decreases with decreasing oxygen abundance and increasing carbon abundance. This results in fewer cloud particles being formed; grains should rain on denser layers and grow to larger sizes than in O-rich atmospheres. However, the inclusion of pebble (Schneider & Bitsch 2021a,b) and collisional (Ogihara et al. 2021) accretion substantially revised this conclusion, showing that the atmospheres of giant planets might be highly enriched in volatile elements (CNO). The very high value of the metallicity obtained for AF Lep b by Zhang et al. (2023) and the moderate one for 51 Eri b by Samland et al. (2017) indeed support this.

Alternatively, we may think that rotation is systematically different in companions and free-floating objects. A higher rotation reduces the efficiency of turbulence and the net speed of vertical motions (Brummell et al. 1996); this in turn implies a higher value for the ratio f_{sed} of the particle sedimentation velocity to the characteristic vertical mixing velocity (Ackerman & Marley 2001). The effect is complex because a higher f_{sed} also implies a higher sedimentation radius, but in general, we expect that a higher value of f_{sed} should correspond to cleaner atmospheres (see also Fig. 15 in Charnay et al. 2018). Hence, a faster rotation should produce cleaner atmospheres. There is no evidence that companions rotate slower than free-floating objects. For instance, the rotational period estimated for β Pic b (8.3 h; Snellen et al. 2014) is actually shorter than the median value of about 1 day found for young (free-floating) brown dwarfs by Scholz (2016), though it is at the lower end of the range of observed values.

We also notice that the origin of free-floating planets is not yet well established (see discussion in Miret-Roig 2023). Several studies indicate that the observed fraction of these objects outnumbers the prediction of cloud turbulent fragmentation (see

e.g. Miret-Roig et al. 2022) and suggest that many were formed in discs around protostars that were later ejected. The colour of free-floating planets may suggest a preference for their formation through gravitational instability. This might indicate that turbulent fragmentation of discs plays a fundamental role in the genesis of free-floating planets, although other channels of formation are also very likely to occur. If this were true, the different dust-settling temperatures of planets might be related to their formation scenario (core accretion vs. disc instability).

5. Conclusions

AF Lep b is the fourth planet discovered through high-contrast imaging in the β Pic moving group, and one of the few extrasolar planets for which dynamical mass and luminosity are available. Consideration of data for this planet strengthens the early conclusion that young massive planets evolve much closer to hot-start models rather than to cold-start ones. The mass-luminosity relation found using the planets in the β Pic moving group is in agreement with the most recent formation and evolution models for giant planets in the core accretion scenario.

Meanwhile, the extensive photometric data gathered recently for sub-stellar objects in young associations and moving groups enables a comparison of the L–T transition occurrences between companions and free-floating objects. These data indicate that the L–T transition occurs at nearly the same magnitude for free-floating objects over quite a large age range (at least up to that of the Hyades) as previously noticed by Liu et al. (2016). The L–T transition is possibly due to the settling of dust in the atmospheres of sub-stellar objects. Since all objects in the mass range between Jupiter and the hydrogen-burning limit share a similar radius with a small range, this means that the settling of dust occurs at a nearly constant temperature of about 1200 K in free-floating objects, rather irrespective of their mass⁵. In contrast, the β Pic moving group planets that are intermediate between the red (dusty) and blue (clean) sequences such as 51 Eri b and AF Lep b are about two magnitudes fainter in the *J* band than free-floating objects of presumably the same mass belonging to the same association. This suggests that the L–T transition – and hence the dust settling – occurs at a lower temperature (about 800–1000 K) in sub-stellar companions than in free-floating objects. This feature is probably not unique to this association. Notably, the sequence of sub-stellar companions features very red (that is cool, dust-rich) objects, which are not observed in free-floating objects.

The reason for this difference between free-floating and companion sub-stellar objects remains unclear, but a very high metallicity for the atmospheres of companions generated by core accretion as possibly found by Zhang et al. (2023) for AF Lep b and Samland et al. (2017) for 51 Eri b is likely. In any case, it signals a systematic difference in their evolution. Further progress in the modelling is needed to explain this observation.

As a final point, we notice that the faintness of the L–T transition for companions – with respect to free-floating objects – may contribute to the low yields of surveys such as the SPHERE infrared survey for exoplanets (SHINE; Vigan et al. 2021) and the Gemini Planet Imager Exoplanet Survey (GPIES;

Nielsen et al. 2019), which were optimised for T-planet detections. This should be taken into account when estimating the frequency of giant planets from these surveys.

Acknowledgements. This work has made use of data from the European Space Agency (ESA) mission *Gaia* (<https://www.cosmos.esa.int/gaia>), processed by the *Gaia* Data Processing and Analysis Consortium (DPAC, <https://www.cosmos.esa.int/web/gaia/dpac/consortium>). Funding for the DPAC has been provided by national institutions, in particular, the institutions participating in the *Gaia* Multilateral Agreement. This research has made use of the SIMBAD database, operated at CDS, Strasbourg, France. D.M., R.G., and S.D. acknowledge the PRIN-INAF 2019 ‘Planetary systems at young ages (PLATEA)’ and ASI-INAF agreement no. 2018-16-HH.0. A.Z. acknowledges support from ANID – Millennium Science Initiative Program – Center Code NCN2021_080. S.M. is supported by the Royal Society as a Royal Society University Research Fellowship (URF-R1-221669). SPHERE is an instrument designed and built by a consortium consisting of IPAG (Grenoble, France), MPIA (Heidelberg, Germany), LAM (Marseille, France), LESIA (Paris, France), Laboratoire Lagrange (Nice, France), INAF-Osservatorio di Padova (Italy), Observatoire de Genève (Switzerland), ETH Zurich (Switzerland), NOVA (Netherlands), ONERA (France) and ASTRON (Netherlands), in collaboration with ESO. SPHERE was funded by ESO, with additional contributions from CNRS (France), MPIA (Germany), INAF (Italy), FINES (Switzerland) and NOVA (The Netherlands). For the purpose of open access, the authors have applied a Creative Commons Attribution (CC BY) licence to any Author Accepted Manuscript version arising from this submission.

References

- Ackerman, A. S., & Marley, M. S. 2001, *ApJ*, 556, 872
 Allard, F., Hauschildt, P. H., Alexander, D. R., Tamanai, A., & Schweitzer, A. 2001, *ApJ*, 556, 357
 Aller, K. M., Kraus, A. L., Liu, M. C., et al. 2013, *ApJ*, 773, 63
 Aller, K. M., Liu, M. C., Magnier, E. A., et al. 2016, *ApJ*, 821, 120
 Bailey, V., Meshkat, T., Reiter, M., et al. 2014, *ApJ*, 780, L4
 Baraffe, I., Chabrier, G., Allard, F., & Hauschildt, P. H. 1998, *A&A*, 337, 403
 Baratella, M., D’Orazi, V., Carraro, G., et al. 2020, *A&A*, 634, A34
 Barrado y Navascués, D., Stauffer, J. R., Song, I., & Caillault, J. P. 1999, *ApJ*, 520, L123
 Barrado y Navascués, D., Stauffer, J. R., & Jayawardhana, R. 2004, *ApJ*, 614, 386
 Baudino, J. L., Bézard, B., Boccaletti, A., et al. 2015, *A&A*, 582, A83
 Bell, C. P. M., Mamajek, E. E., & Naylor, T. 2015, *MNRAS*, 454, 593
 Berardo, D., Cumming, A., & Marleau, G.-D. 2017, *ApJ*, 834, 149
 Best, W. M. J., Liu, M. C., Magnier, E. A., & Dupuy, T. J. 2020, *AJ*, 159, 257
 Binks, A. S., & Jeffries, R. D. 2014, *MNRAS*, 438, L11
 Bohn, A. J., Kenworthy, M. A., Ginski, C., et al. 2020a, *MNRAS*, 492, 431
 Bohn, A. J., Kenworthy, M. A., Ginski, C., et al. 2020b, *ApJ*, 898, L16
 Bohn, A. J., Ginski, C., Kenworthy, M. A., et al. 2021, *A&A*, 648, A73
 Bohn, A. J., Ginski, C., Kenworthy, M. A., et al. 2022, *A&A*, 657, A53
 Booth, M., del Burgo, C., & Hambaryan, V. V. 2021, *MNRAS*, 500, 5552
 Bouy, H., Tamura, M., Barrado, D., et al. 2022, *A&A*, 664, A111
 Bowler, B. P., Liu, M. C., Shkolnik, E. L., et al. 2012, *ApJ*, 753, 142
 Bowler, B. P., Liu, M. C., Mawet, D., et al. 2017, *AJ*, 153, 18
 Brummell, N. H., Hurlburt, N. E., & Toomre, J. 1996, *ApJ*, 473, 494
 Burgasser, A. J. 2007, *ApJ*, 659, 655
 Burrows, A., Sudarsky, D., & Hubeny, I. 2006, *ApJ*, 640, 1063
 Chabrier, G., Baraffe, I., Allard, F., & Hauschildt, P. 2000, *ApJ*, 542, 464
 Charnay, B., Bézard, B., Baudino, J. L., et al. 2018, *ApJ*, 854, 172
 Chauvin, G., Desidera, S., Lagrange, A. M., et al. 2017, *A&A*, 605, A9
 Chauvin, G., Gratton, R., Bonnefoy, M., et al. 2018, *A&A*, 617, A76
 Cheetham, A., Bonnefoy, M., Desidera, S., et al. 2018, *A&A*, 615, A160
 Couture, D., Gagné, J., & Doyon, R. 2023, *ApJ*, 946, 6
 De Rosa, R. J., Rameau, J., Patience, J., et al. 2016, *ApJ*, 824, 121
 De Rosa, R. J., Nielsen, E. L., Wahhaj, Z., et al. 2023, *A&A*, 672, A94
 Delorme, P., Gagné, J., Girard, J. H., et al. 2013, *A&A*, 553, A5
 Delorme, P., Meunier, N., Albert, D., et al. 2017, in *SF2A-2017: Proceedings of the Annual meeting of the French Society of Astronomy and Astrophysics*, eds. C. Reylé, P. Di Matteo, F. Herpin, et al., 347
 Desrochers, M.-E., Artigau, É., Gagné, J., et al. 2018, *ApJ*, 852, 55
 Dupuy, T. J., & Liu, M. C. 2012, *ApJS*, 201, 19
 Dupuy, T. J., & Liu, M. C. 2017, *ApJS*, 231, 15
 Dupuy, T. J., Brandt, G. M., & Brandt, T. D. 2022, *MNRAS*, 509, 4411
 Faherty, J. K., Riedel, A. R., Cruz, K. L., et al. 2016, *ApJS*, 225, 10
 Filippazzo, J. C., Rice, E. L., Faherty, J., et al. 2015, *ApJ*, 810, 158
 Franson, K., & Bowler, B. P. 2023, *AJ*, 165, 246

⁵ In principle correct the bolometric correction should also be considered here. However, as shown by Fig. 11, the L–T transition of the free-floating objects occurs in a rather narrow range of temperatures between 1100 and 1200 K. The range is even more restricted when we use temperatures obtained considering appropriate bolometric corrections.

- Franson, K., Bowler, B. P., Zhou, Y., et al. 2023, *ApJ*, **950**, L19
- Gagné, J., Faherty, J. K., Cruz, K. L., et al. 2015, *ApJS*, **219**, 33
- Gagné, J., Fontaine, G., Simon, A., & Faherty, J. K. 2018a, *ApJ*, **861**, L13
- Gagné, J., Mamajek, E. E., Malo, L., et al. 2018b, *ApJ*, **856**, 23
- Gizis, J. E. 2002, *ApJ*, **575**, 484
- Gizis, J. E., Allers, K. N., Liu, M. C., et al. 2015, *ApJ*, **799**, 203
- Helling, C., Woitke, P., Rimmer, P. B., et al. 2014, *Life*, **4**, 142
- Hurt, S. A., Liu, M. C., Zhang, Z., et al. 2024, *ApJ*, **961**, 121
- Ireland, M. J., Kraus, A., Martinache, F., Law, N., & Hillenbrand, L. A. 2011, *ApJ*, **726**, 113
- Janson, M., Jayawardhana, R., Girard, J. H., et al. 2012, *ApJ*, **758**, L2
- Janson, M., Asensio-Torres, R., André, D., et al. 2019, *A&A*, **626**, A99
- Janson, M., Gratton, R., Rodet, L., et al. 2021, *Nature*, **600**, 231
- Keppeler, M., Benisty, M., Müller, A., et al. 2018, *A&A*, **617**, A44
- Kerr, R., Kraus, A. L., Murphy, S. J., et al. 2022, *ApJ*, **941**, 143
- Knapp, G. R., Leggett, S. K., Fan, X., et al. 2004, *AJ*, **127**, 3553
- Kraus, A. L., Ireland, M. J., Cieza, L. A., et al. 2014, *ApJ*, **781**, 20
- Lafrenière, D., Jayawardhana, R., Janson, M., et al. 2011, *ApJ*, **730**, 42
- Langlois, M., Gratton, R., Lagrange, A. M., et al. 2021, *A&A*, **651**, A71
- Liu, M. C., Magnier, E. A., Deacon, N. R., et al. 2013, *ApJ*, **777**, L20
- Liu, M. C., Dupuy, T. J., & Allers, K. N. 2016, *ApJ*, **833**, 96
- Lodieu, N., Hambly, N. C., & Jameson, R. F. 2006, *MNRAS*, **373**, 95
- Maire, A. L., Bonnefoy, M., Ginski, C., et al. 2016, *A&A*, **587**, A56
- Majidi, F. Z., Desidera, S., Alcalá, J. M., et al. 2020, *A&A*, **644**, A169
- Malo, L., Doyon, R., Feiden, G. A., et al. 2014, *ApJ*, **792**, 37
- Mamajek, E. E., & Bell, C. P. M. 2014, *MNRAS*, **445**, 2169
- Marley, M. S., & Robinson, T. D. 2015, *ARA&A*, **53**, 279
- Marley, M. S., Fortney, J. J., Hubickyj, O., Bodenheimer, P., & Lissauer, J. J. 2007, *ApJ*, **655**, 541
- Marley, M. S., Saumon, D., & Goldblatt, C. 2010, *ApJ*, **723**, L117
- McCarthy, K., & Wilhelm, R. J. 2014, *AJ*, **148**, 70
- Mentuch, E., Brandeker, A., van Kerkwijk, M. H., Jayawardhana, R., & Hauschildt, P. H. 2008, *ApJ*, **689**, 1127
- Mesa, D., Keppler, M., Cantalloube, F., et al. 2019, *A&A*, **632**, A25
- Mesa, D., Gratton, R., Kervella, P., et al. 2023, *A&A*, **672**, A93
- Miret-Roig, N. 2023, *Ap&SS*, **368**, 17
- Miret-Roig, N., Galli, P. A. B., Brandner, W., et al. 2020, *A&A*, **642**, A179
- Miret-Roig, N., Bouy, H., Raymond, S. N., et al. 2022, *Nat. Astron.*, **6**, 89
- Mollière, P., Wardenier, J. P., van Boekel, R., et al. 2019, *A&A*, **627**, A67
- Mordasini, C., Marleau, G. D., & Mollière, P. 2017, *A&A*, **608**, A72
- Morley, C. V., Fortney, J. J., Marley, M. S., et al. 2012, *ApJ*, **756**, 172
- Naud, M.-E., Artigau, É., Malo, L., et al. 2014, *ApJ*, **787**, 5
- Neuhäuser, R., Ginski, C., Schmidt, T. O. B., & Mugrauer, M. 2011, *MNRAS*, **416**, 1430
- Nielsen, E. L., De Rosa, R. J., Macintosh, B., et al. 2019, *AJ*, **158**, 13
- Nowak, M., Lacour, S., Lagrange, A. M., et al. 2020, *A&A*, **642**, A2
- Ogihara, M., Hori, Y., Kunitomo, M., & Kurosaki, K. 2021, *A&A*, **648**, A1
- Patience, J., King, R. R., De Rosa, R. J., et al. 2012, *A&A*, **540**, A85
- Pecaut, M. J., & Mamajek, E. E. 2016, *MNRAS*, **461**, 794
- Samland, M., Mollière, P., Bonnefoy, M., et al. 2017, *A&A*, **603**, A57
- Saumon, D., & Marley, M. S. 2008, *ApJ*, **689**, 1327
- Schneider, A. D., & Bitsch, B. 2021a, *A&A*, **654**, A71
- Schneider, A. D., & Bitsch, B. 2021b, *A&A*, **654**, A72
- Schneider, A. C., Cushing, M. C., Kirkpatrick, J. D., et al. 2014, *AJ*, **147**, 34
- Schneider, A. C., Windsor, J., Cushing, M. C., Kirkpatrick, J. D., & Shkolnik, E. L. 2017, *AJ*, **153**, 196
- Schneider, A. C., Shkolnik, E. L., Allers, K. N., et al. 2019, *AJ*, **157**, 234
- Schneider, A. C., Burgasser, A. J., Bruursema, J., et al. 2023, *ApJ*, **943**, L16
- Scholz, A. 2016, arXiv e-prints [arXiv:1610.06428]
- Shkolnik, E. L., Allers, K. N., Kraus, A. L., Liu, M. C., & Flagg, L. 2017, *AJ*, **154**, 69
- Snellen, I. A. G., Brandl, B. R., de Kok, R. J., et al. 2014, *Nature*, **509**, 63
- Spiegel, D. S., & Burrows, A. 2012, *ApJ*, **745**, 174
- Squicciarini, V., Gratton, R., Janson, M., et al. 2022, *A&A*, **664**, A9
- Tremblin, P., Amundsen, D. S., Chabrier, G., et al. 2016, *ApJ*, **817**, L19
- Ujjwal, K., Kartha, S. S., Mathew, B., Manoj, P., & Narang, M. 2020, *AJ*, **159**, 166
- Uyama, T., Currie, T., Hori, Y., et al. 2020, *AJ*, **159**, 40
- Vigan, A., Fontanive, C., Meyer, M., et al. 2021, *A&A*, **651**, A72
- Viswanath, G., Janson, M., Gratton, R., et al. 2023, *A&A*, **675**, A54
- Vos, J., Allers, K., Apai, D., et al. 2019, *BAAS*, **51**, 253
- Wagner, K., Apai, D., Kasper, M., et al. 2020, *ApJ*, **902**, L6
- Wood, M., & Mann, A. 2023, in *American Astronomical Society Meeting Abstracts*, **55**, 402.10
- Zhang, Z., Liu, M. C., Best, W. M. J., Dupuy, T. J., & Siverd, R. J. 2021, *ApJ*, **911**, 7
- Zhang, Z., Mollière, P., Hawkins, K., et al. 2023, *AJ*, **166**, 198
- Zuckerman, B., Bessell, M. S., Song, I., & Kim, S. 2006, *ApJ*, **649**, L115
- Zurlo, A., Vigan, A., Galicher, R., et al. 2016, *A&A*, **587**, A57
- Zurlo, A., Goździewski, K., Lazzoni, C., et al. 2022, *A&A*, **666**, A133

Appendix A: Photometry of sub-stellar objects

Table A.1. Photometry for sub-stellar objects in the BPMG

2MASS/Others	prob %	par mas	<i>J</i> mag	<i>H</i> mag	<i>K</i> mag	<i>M_J</i> mag	<i>M_H</i> mag	<i>M_K</i> mag	<i>J - K</i> mag	Source
Companions										
51 Eri b b	8.9	33.44	19.779 ± 0.200	19.489 ± 0.210	18.489 ± 0.14	17.40 ± 0.20	17.11 ± 0.21	16.11 ± 0.14	1.29 ± 0.24	Samland et al. (2017)
AF Lep b b	99.9	37.25	19.644 ± 0.770	18.964 ± 0.610	16.644 ± 0.40	17.50 ± 0.77	16.82 ± 0.61	14.50 ± 0.40	3.00 ± 0.87	Mesa et al. (2023)
beta Pic b b	99.9	51.44	14.250 ± 0.200	13.223 ± 0.200	12.473 ± 0.05	12.81 ± 0.20	11.78 ± 0.20	11.03 ± 0.05	1.78 ± 0.21	Langlois et al. (2021)
beta Pic c c	99.9	51.44			14.343 ± 0.10			12.90 ± 0.10		Nowak et al. (2020)
PZ Tel B B	97.2	21.16	12.470 ± 0.100	11.930 ± 0.100	11.530 ± 0.09	9.10 ± 0.1	8.56 ± 0.10	8.16 ± 0.09	0.94 ± 0.13	Maire et al. (2016)
eta Tel B B	77.1	20.60	12.060 ± 0.190	11.750 ± 0.100	11.600 ± 0.100	8.87 ± 0.1	8.52 ± 0.10	7.87 ± 0.10	1.00 ± 0.14	Neuhäuser et al. (2011)
Free floating objects										
J00305194-3808292	82.5	22.22	17.180 ± 0.231	16.062 ± 0.175	15.172 ± 0.162	13.91 ± 0.231	12.80 ± 0.18	11.91 ± 0.16	2.01 ± 0.28	Schneider et al. (2017)
J00440332+0228112	75.3	31.95	16.997 ± 0.187	15.822 ± 0.169	14.876 ± 0.105	14.52 ± 0.187	13.34 ± 0.17	12.40 ± 0.11	2.12 ± 0.21	Schneider et al. (2017)
J01073866-1314134	47.4	35.71	16.710 ± 0.131	15.577 ± 0.120	14.625 ± 0.095	14.47 ± 0.131	13.34 ± 0.12	12.39 ± 0.10	2.09 ± 0.16	Schneider et al. (2017)
J03350208+2342356	98.3	19.72	12.250 ± 0.021	11.655 ± 0.022	11.261 ± 0.017	8.73 ± 0.021	8.13 ± 0.02	7.74 ± 0.02	0.99 ± 0.03	Shkolnik et al. (2017)
J04433761+0002051	99.9	47.62	12.507 ± 0.026	11.804 ± 0.024	11.216 ± 0.021	10.90 ± 0.026	10.19 ± 0.02	9.60 ± 0.03	1.29 ± 0.03	Shkolnik et al. (2017)
2MASS J0453264-175154	99.2	33.06	15.142 ± 0.035	14.060 ± 0.035	13.466 ± 0.035	12.74 ± 0.035	11.66 ± 0.04	11.06 ± 0.04	1.68 ± 0.05	Hurt et al. (2024)
J05361998-1920396	79.3	25.60	15.768 ± 0.075	14.693 ± 0.071	13.854 ± 0.062	12.81 ± 0.075	11.73 ± 0.07	10.90 ± 0.06	1.91 ± 0.10	Gagné et al. (2015)
J08195820-0335266	84.2	72.00	14.991 ± 0.044	14.638 ± 0.057	14.586 ± 0.105	14.28 ± 0.044	13.92 ± 0.06	13.87 ± 0.11	0.40 ± 0.11	Zhang et al. (2021)
J09462782-4457408	99.0	21.44	10.876 ± 0.026	10.337 ± 0.022	9.992 ± 0.021	7.53 ± 0.026	6.99 ± 0.02	6.65 ± 0.02	0.88 ± 0.03	Schneider et al. (2019)
J10134260-2759586	5.2	24.38	12.261 ± 0.028	11.626 ± 0.023	11.252 ± 0.021	9.20 ± 0.028	8.56 ± 0.02	8.19 ± 0.02	1.01 ± 0.04	Gizis (2002)
J19082195-1603249	81.7	14.35	12.198 ± 0.024	11.667 ± 0.024	11.402 ± 0.023	7.98 ± 0.024	7.45 ± 0.02	7.19 ± 0.02	0.80 ± 0.03	Shkolnik et al. (2017)
J19355595-2846343	99.0	17.50	13.953 ± 0.027	13.180 ± 0.022	12.712 ± 0.029	10.17 ± 0.027	9.39 ± 0.02	8.93 ± 0.03	1.24 ± 0.04	Shkolnik et al. (2017)
J20004841-7523070	99.9	34.01	12.734 ± 0.026	11.967 ± 0.027	11.511 ± 0.026	10.39 ± 0.026	9.63 ± 0.03	9.17 ± 0.03	1.22 ± 0.04	Shkolnik et al. (2017)
J20135152-2806020	99.7	21.05	14.240 ± 0.030	13.461 ± 0.028	12.944 ± 0.027	10.86 ± 0.030	10.08 ± 0.03	9.56 ± 0.03	1.30 ± 0.04	Shkolnik et al. (2017)
J20153059-4215419	57.1	25.64	17.648 ± 0.317	16.233 ± 0.151	15.366 ± 0.145	14.69 ± 0.317	13.28 ± 0.15	12.41 ± 0.15	2.28 ± 0.35	Schneider et al. (2017)
J20334670-3733443	99.6	30.62	10.848 ± 0.022	10.297 ± 0.024	9.996 ± 0.021	8.28 ± 0.022	7.73 ± 0.02	7.43 ± 0.02	0.85 ± 0.03	Gagné et al. (2015)
2MASS J21043128-0939217	67.6	18.60	15.851 ± 0.072	14.852 ± 0.062	14.415 ± 0.075	12.20 ± 0.072	11.20 ± 0.06	10.76 ± 0.08	1.44 ± 0.10	Hurt et al. (2024)
J21171431-2940034	99.4	52.40	15.601 ± 0.060	14.527 ± 0.043	14.150 ± 0.066	14.20 ± 0.060	13.12 ± 0.04	12.75 ± 0.07	1.45 ± 0.09	Best et al. (2020)
J21140802-2251358	99.0	45.10	16.706 ± 0.195	15.720 ± 0.170	14.740 ± 0.118	14.98 ± 0.195	13.99 ± 0.17	13.01 ± 0.12	1.97 ± 0.23	Liu et al. (2013)
J22081363+2921215	13.5	24.30	15.797 ± 0.085	14.793 ± 0.071	14.148 ± 0.073	12.73 ± 0.085	11.72 ± 0.07	11.08 ± 0.07	1.65 ± 0.11	Shkolnik et al. (2017)
J22334687-2950101	44.7	19.19	12.941 ± 0.024	12.324 ± 0.023	11.971 ± 0.024	9.36 ± 0.024	8.74 ± 0.02	8.39 ± 0.02	0.97 ± 0.03	Shkolnik et al. (2017)
J22443167+2043433	99.7	58.70	16.476 ± 0.140	14.999 ± 0.066	14.022 ± 0.073	15.32 ± 0.140	13.84 ± 0.07	12.87 ± 0.07	2.45 ± 0.16	Liu et al. (2016)
J22533287-2539475	48.2	23.26	17.152 ± 0.214	15.752 ± 0.148	15.075 ± 0.144	13.99 ± 0.214	12.59 ± 0.15	11.91 ± 0.14	2.08 ± 0.26	Schneider et al. (2017)
WISE J225540.75-311842.0	98.7	71.00	17.334 ± 0.020	17.660 ± 0.050	17.420 ± 0.050	16.59 ± 0.020	16.92 ± 0.05	16.68 ± 0.05	-0.09 ± 0.05	Zhang et al. (2021)
CFBDS J232304-015232	89.1	30.20	17.230 ± 0.030	17.460 ± 0.040	17.300 ± 0.030	14.63 ± 0.030	14.86 ± 0.04	14.70 ± 0.03	-0.07 ± 0.04	Zhang et al. (2021)
J23355015-3401477	98.6	26.76	11.639 ± 0.026	11.062 ± 0.026	10.758 ± 0.021	8.78 ± 0.026	8.20 ± 0.03	7.90 ± 0.02	0.88 ± 0.03	Shkolnik et al. (2017)
J23542220-0811289	94.3	26.32	17.255 ± 0.230	15.962 ± 0.150	14.790 ± 0.120	14.36 ± 0.230	13.06 ± 0.15	11.89 ± 0.12	2.47 ± 0.26	Schneider et al. (2017)
CWISE J050626.96+073842.4	82.3	31.25	18.758 ± 0.102		15.513 ± 0.022	16.23 ± 0.102		12.99 ± 0.02	3.25 ± 0.10	Schneider et al. (2023)

^a Photometric parallax

Table A.2. Cont...

2MASS/Others	memb %	par mas	J mag	H mag	K mag	M_J mag	M_H mag	M_K mag	$J - K$ mag	Source
Carina Near										
PSO J004.6359+56.8370	90.8	47.00	16.220 ± 0.020	16.240 ± 0.020	16.130 ± 0.020	14.58 ± 0.02	14.60 ± 0.02	14.49 ± 0.02	0.09 ± 0.03	Zhang et al. (2021)
Koenigstuhl 1B	98.5	37.93	13.521 ± 0.025	12.809 ± 0.025	12.304 ± 0.025	11.42 ± 0.03	10.70 ± 0.03	10.20 ± 0.03	1.22 ± 0.04	Hurt et al. (2024)
WISE J003110.04+574936.3	97.5	71.00	14.950 ± 0.040	13.780 ± 0.040	13.215 ± 0.029	14.21 ± 0.04	13.04 ± 0.04	12.47 ± 0.03	1.74 ± 0.05	Hurt et al. (2024)
SIMP J013656.5+093347.3	95.6	163.70	13.252 ± 0.002	12.809 ± 0.002	12.585 ± 0.002	14.32 ± 0.00	13.88 ± 0.00	13.66 ± 0.00	0.67 ± 0.00	Zhang et al. (2021)
J01033203+1935361	59.6	46.90	16.288 ± 0.080	14.897 ± 0.056	14.149 ± 0.059	14.64 ± 0.08	13.25 ± 0.06	12.50 ± 0.06	2.14 ± 0.10	Schneider et al. (2017)
WISE J031624.35+430709.1	95.4	73.30	19.470 ± 0.040	19.700 ± 0.090		18.80 ± 0.040	19.03 ± 0.09			Zhang et al. (2021)
J04371868-5509449	88.2	28.57	16.985 ± 0.192	15.583 ± 0.157	14.640 ± 0.098	14.26 ± 0.19	12.86 ± 0.16	11.92 ± 0.10	2.35 ± 0.22	Schneider et al. (2017)
J04590034-2853396	70.2	26.32	17.429 ± 0.282	16.375 ± 0.249	15.318 ± 0.197	14.53 ± 0.28	13.48 ± 0.25	12.42 ± 0.20	2.11 ± 0.34	Schneider et al. (2017)
J07235265-3309446	90.7	30.83	15.743 ± 0.059	14.471 ± 0.043	13.715 ± 0.047	13.19 ± 0.06	11.92 ± 0.04	11.16 ± 0.05	2.03 ± 0.08	Schneider et al. (2017)
DENIS-P J090957.1-065806	99.5	40.56	13.890 ± 0.024	13.090 ± 0.021	12.539 ± 0.026	11.93 ± 0.02	11.13 ± 0.02	10.58 ± 0.03	1.35 ± 0.04	Hurt et al. (2024)
2MASSW J0928397-160312	99.1	31.73	15.322 ± 0.043	14.292 ± 0.037	13.615 ± 0.051	12.83 ± 0.04	11.80 ± 0.04	11.12 ± 0.05	1.71 ± 0.07	Hurt et al. (2024)
2MASS J1010148-040649	98.7	55.00	15.508 ± 0.059	14.385 ± 0.037	13.619 ± 0.046	14.21 ± 0.06	13.09 ± 0.04	12.32 ± 0.05	1.89 ± 0.07	Hurt et al. (2024)
J11544223-3400390	95.9	26.06	14.195 ± 0.033	13.331 ± 0.028	12.851 ± 0.033	11.27 ± 0.03	10.41 ± 0.03	9.93 ± 0.03	1.34 ± 0.05	Gagné et al. (2015)
2MASSW J1326201-272937	87.9	54.70	15.847 ± 0.071	14.741 ± 0.058	13.852 ± 0.054	14.54 ± 0.07	13.43 ± 0.06	12.54 ± 0.05	2.00 ± 0.09	Hurt et al. (2024)
J14413716-0945590	58.0	32.51	14.020 ± 0.029	13.190 ± 0.031	12.661 ± 0.030	11.58 ± 0.03	10.75 ± 0.03	10.22 ± 0.03	1.36 ± 0.04	Liu et al. (2016) ^b
J15530228+1532369	89.6	75.10	15.825 ± 0.071	15.939 ± 0.163	15.507 ± 0.182	15.20 ± 0.07	15.32 ± 0.16	14.89 ± 0.18	0.32 ± 0.20	Zhang et al. (2021)
Lower Centaurus-Crux										
HD95086 b	80.8	11.57	22.290 ± 0.450	20.270 ±	18.990 ± 0.100	17.61 ± 0.45	15.59 ±	14.31 ± 0.10	3.30 ± 0.46	De Rosa et al. (2016) Chauvin et al. (2018)
TYC 8984-2245-1 b	99.9	9.11		18.77±0.11	17.912±0.11		13.57 ± 0.11	12.71±0.11		Bohn et al. (2021)
TYC 8986-3110-1 B	99.9	9.21	13.158 ± 0.047	12.610 ± 0.042	12.197 ± 0.390	7.98 ± 0.05	7.43 ± 0.04	7.02 ± 0.39	0.96 ± 0.39	Bohn et al. (2022)
HD106906 b	99.8	9.77	17.600 ± 0.300		15.460 ± 0.060	12.55 ± 0.30		10.41 ± 0.06	2.14± 0.31	Bailey et al. (2014)
TYC 8654-2791-1 B	99.8	9.82	13.693 ± 0.043	13.124 ± 0.040	12.706 ± 0.035	8.65 ± 0.04	8.08 ± 0.04	7.67 ± 0.04	0.99 ± 0.06	Bohn et al. (2022)
TYC 9245-535-1 B	98.5	10.07	12.387 ± 0.083	11.853 ± 0.218	11.461 ± 0.078	7.40 ± 0.08	6.87 ± 0.22	6.48 ± 0.08	0.93 ± 0.11	Bohn et al. (2022)
HIP64892 B	74.0	8.36		14.119 ± 0.170	13.512 ± 0.170		8.73 ± 0.17	8.17 ± 0.17		Cheetham et al. (2018)
TYC 8252-533-1 B	80.5	7.71	13.540 ± 0.160	12.720 ± 0.090	12.420 ± 0.050	7.98 ± 0.16	7.16 ± 0.09	6.86 ± 0.05	1.12 ± 0.17	Bohn et al. (2022)
J13242119-5129503	98.0	8.15	14.594 ± 0.029	14.036 ± 0.041	13.627 ± 0.047	9.15 ± 0.03	8.59 ± 0.04	8.18 ± 0.05	0.97 ± 0.06	Majidi et al. (2020)
HIP65423 B	96.9	8.40		12.930 ± 0.060	12.510 ± 0.120		7.55 ± 0.06	7.13 ± 0.12		Janson et al. (2012)
HIP65426 b	91.4	9.30	18.940 ± 0.110	17.640 ± 0.120	16.900 ± 0.330	13.78 ± 0.11	12.48 ± 0.12	11.74 ± 0.33	2.04 ± 0.35	Chauvin et al. (2017)
TYC 8998-760-1 c	99.1	10.54	21.532 ± 0.150		18.192 ± 0.090	16.65 ± 0.15		13.31 ± 0.09	3.34 ± 0.17	Bohn et al. (2020b)
TYC 8998-760-1 b	99.1	10.54	15.730 ± 0.080	14.870 ± 0.080	14.250 ± 0.040	10.84 ± 0.08	9.98 ± 0.08	9.36 ± 0.04	1.48 ± 0.09	Bohn et al. (2020a)
HIP65517 B	69.2	10.24		12.850± 0.030	12.540± 0.030		7.90± 0.030	7.59± 0.030		Janson et al. (2012)
Upper Centaurus-Lupus										
IRXS J131752.0-505845 B	69.4	6.36	14.784 ± 0.036	14.086 ± 0.031	13.776 ± 0.052	8.80 ± 0.04	8.10 ± 0.03	7.79 ± 0.05	1.01 ± 0.06	Bohn et al. (2022)
PDS-70 b	98.7	8.90	20.250 ± 0.150	18.160	16.280 ± 0.280	15.00 ± 0.15	12.91	11.03 ± 0.28	3.97 ± 0.32	Kepler et al. (2018)
PDS-70 c	98.7	8.90	22.470 ± 0.250	19.110	17.744 ± 0.140	17.22 ± 0.25	13.86	12.49 ± 0.14	4.73 ± 0.29	Mesa et al. (2019)
b Cen b	99.9	9.62	17.810 ± 0.250		16.344 ± 0.060	12.82 ± 0.25		11.26 ± 0.06	1.56 ± 0.26	Janson et al. (2021)
J14571503-3543505	99.6	9.49	14.131 ± 0.027	13.495 ± 0.029	13.106 ± 0.036	9.02 ± 0.03	8.38 ± 0.03	7.99 ± 0.04	1.03 ± 0.05	Majidi et al. (2020)
J15113968-3248560 B	95.1	7.05	13.578 ± 0.027	13.000 ± 0.025	12.720 ± 0.033	7.82 ± 0.03	7.24 ± 0.03	6.96 ± 0.03	0.86 ± 0.04	Bohn et al. (2022)
HIP74752 B	99.9	7.64	13.055 ± 0.002		12.783 ± 0.003	7.47 ± 0.00		7.20 ± 0.00	0.27 ± 0.00	Gaia, VISTA
HIP74865 B	99.1	8.09	12.544 ± 0.023	11.933 ± 0.024	11.641 ± 0.021	7.08 ± 0.02	6.47 ± 0.02	6.18 ± 0.02	0.90 ± 0.03	Langlois et al. (2021)
HIP75056 B	99.9	7.94	14.680 ± 0.250	14.500 ± 0.250	14.080 ± 0.100	9.18 ± 0.25	9.00 ± 0.25	8.58 ± 0.10	0.60 ± 0.27	Wagner et al. (2020)
GQ Lup B	99.4	6.49	14.900 ± 0.110	13.790 ± 0.300	13.340 ± 0.130	8.96 ± 0.11	7.85 ± 0.30	7.40 ± 0.13	1.56 ± 0.17	Patience et al. (2012)
J15545141-3154463 B	19.6	7.10	13.015 ± 0.074	11.804 ± 0.077	11.159 ± 0.034	7.27 ± 0.11	6.06 ± 0.08	5.42 ± 0.03	1.86 ± 0.12	Bohn et al. (2022)
NQ Lup B	99.2	7.81	13.011 ± 0.065	12.479 ± 0.086	12.133 ± 0.053	7.47 ± 0.07	6.94 ± 0.09	6.60 ± 0.05	0.88 ± 0.08	Bohn et al. (2022)
TYC 7851-426-1 B	86.6	6.41	15.459 ± 0.064	14.262 ± 0.036	13.305 ± 0.042	9.49 ± 0.06	8.30 ± 0.04	7.34 ± 0.04	2.15 ± 0.08	Bohn et al. (2022)
HIP81208 B	95.4	6.75	14.290 ± 0.140	13.920 ± 0.150	13.490 ± 0.090	8.44 ± 0.03	8.07 ± 0.15	7.64 ± 0.09	0.80 ± 0.09	Viswanath et al. (2023)
mu2 Sco c	99.5	6.88	17.320		15.690 ± 0.380	11.51		9.88 ± 0.38	1.63 ± 0.38	Squicciarini et al. (2022)
mu2 Sco b	99.5	6.88			15.482± 0.320			9.67 ± 0.32		Squicciarini et al. (2022)
GSC 06214-00210 b	56.8	9.19	16.298 ± 0.080	15.550 ± 0.070	14.932 ± 0.060	11.12 ± 0.03	10.37 ± 0.07	9.75 ± 0.06	1.37 ± 0.07	Ireland et al. (2011)
Upper Scorpius										
HIP77900 B	97.6	6.71	15.070 ± 0.010	14.520 ± 0.010	14.040 ± 0.010	9.20 ± 0.01	8.65 ± 0.01	8.17 ± 0.01	1.03 ± 0.01	Aller et al. (2013)
HIP78530 B	99.9	8.25	15.060 ± 0.050	14.390 ± 0.040	14.170 ± 0.040	9.64 ± 0.05	8.97 ± 0.04	8.75 ± 0.04	0.89 ± 0.06	Lafrenière et al. (2011)
USco 1602.8-2401 B	99.7	6.80	12.542 ± 0.061	11.960 ± 0.060	11.619 ± 0.045	6.70 ± 0.06	6.12 ± 0.06	5.78 ± 0.05	0.92 ± 0.08	Aller et al. (2013)
J16065795-2743094 B	97.5	6.49	13.748 ± 0.022	13.084 ± 0.023	12.730 ± 0.026	7.81 ± 0.02	7.15 ± 0.02	6.79 ± 0.03	1.02 ± 0.03	Bohn et al. (2022)
J16083436-1911563 B	99.8	8.38	13.125 ± 0.026	12.494 ± 0.027	12.172 ± 0.025	7.74 ± 0.03	7.11 ± 0.03	6.79 ± 0.03	0.95 ± 0.04	Bohn et al. (2022)
TYC 6784-39-1 B	99.5	7.28	14.139 ± 0.039	13.452 ± 0.030	13.034 ± 0.034	8.45 ± 0.04	7.76 ± 0.03	7.34 ± 0.03	1.11 ± 0.05	Bohn et al. (2022)
HIP79098 B	98.9	6.83	15.830 ± 0.210	14.900 ± 0.210	14.150 ± 0.100	10.00 ± 0.21	9.07 ± 0.21	8.32 ± 0.10	1.68 ± 0.23	Janson et al. (2019)
IRXS J161021.2-190408 B	99.9	7.48	12.970 ± 0.050	12.348 ± 0.055	11.925 ± 0.041	7.34 ± 0.05	6.72 ± 0.06	6.29 ± 0.04	1.05 ± 0.06	Bohn et al. (2022)
USco 161248.9-180052 B	99.3	6.52		13.730 ± 0.010	13.200 ± 0.010		7.80 ± 0.01	7.27 ± 0.01		Aller et al. (2013)
J16265280-2343127 B	98.3	7.25	13.541 ± 0.026	12.623 ± 0.023	12.049 ± 0.026	7.84 ± 0.03	6.92 ± 0.02	6.35 ± 0.03	1.49 ± 0.04	Bohn et al. (2022)
USco J1610-1913 B	99.9	7.29	13.890 ± 0.080	13.280 ± 0.070	12.790 ± 0.060	8.20 ± 0.08	7.59 ± 0.07	7.10 ± 0.06	1.10 ± 0.10	Kraus et al. (2014)
IRXS J160929.1-210524 b	99.9	7.24	17.900 ± 0.130	16.870 ± 0.090	16.230 ± 0.060	12.20 ± 0.13	11.17 ± 0.09	10.53 ± 0.03	1.67 ± 0.13	Ireland et al. (2011)

^a Photometric parallax

^b Binary

Appendix B: Masses of young sub-stellar objects with AMES models**Table B.1.** Masses of sub-stellar objects with ages in the range 10-200 Myr derived using AMES models

Name	Age Myr	T_{eff} (BC) K	T_{eff} (remap) K	r	Mass M_{Jup}
Companions					
51 Eri b	21	786± 8	746± 10	0.11± 0.11	4.11± 0.30
AF Lep b	21	950± 27	940± 9	0.29± 0.20	5.62± 0.36
beta Pic b	21	1711± 63	1570± 32	0.71± 0.16	11.83± 0.91
GSC08047-00232 B	36	1988± 48	1975± 66	0.49± 0.30	19.77± 1.14
HR8799 b	36	1013± 35	1012± 18	0.46± 0.09	7.24± 0.58
HR8799 c	36	1205± 52	1172± 22	0.50± 0.09	8.71± 0.71
HR8799 d	36	1205± 52	1173± 22	0.49± 0.08	8.82± 0.66
HR8799 e	36	1216± 53	1182± 6	0.47± 0.09	8.87± 0.62
kap And b	36	1776± 61	1699± 41	0.59± 0.08	15.03± 0.66
HD95086 b	16	978± 31	982± 6	0.57± 0.11	5.37± 0.61
HD106906 b	13	1897± 54	2078± 0	1.08± 0.00	33.35±34.76
HIP65426 b	16	1514± 64	1406± 54	0.66± 0.22	10.02± 9.50
TYC 8998-760-1 c	16	1151± 48	1120± 0	0.58± 0.00	6.36± 0.64
TYC 8998-760-1 b	16	2237± 20	2768± 572	0.45± 1.14	76.91± 9.53
ROXs 12B	10	2534± 30	2721± 550	-0.02± 1.00	85.20± 1.89
ROXs 42B	10	2285± 13	2656± 635	0.06± 1.10	84.40± 2.28
b Cen b	16	1646± 64	1571± 0	0.47± 0.00	11.53± 8.17
GSC 06214-00210 b	16	2107± 36	2244± 572	0.54± 1.17	24.86±21.85
1RXS J160929.1-210524 b	10	1879± 55	2003± 310	0.42± 1.16	37.89±36.24
J02192210-3925225 B	37	1779± 60	1695± 52	0.67± 0.17	15.81± 8.74
J01033563-5515561 B	37	1953± 50	1819± 273	1.04± 0.08	17.03± 1.47
AB Pic b	28	1827± 58	1647± 78	0.96± 0.23	14.54± 8.22
CD-35 2722 B	137	1944± 51	2065± 55	1.09± 0.03	37.29± 2.18
J22362452+4751425 B	137	1201± 52	1205± 27	0.47± 0.02	15.28± 1.11
J22501512+2325342 B	137	1691± 63	1748± 40	0.74± 0.06	26.69± 2.36
1RXS J235133.3+312720 B	137	1791± 60	1802± 44	1.05± 0.04	27.80± 1.67
GU Psc b	137	1025± 36	1075± 19	0.08± 0.02	13.29± 1.01
Free floating objects					
J00305194-3808292	21	1470± 64	1377± 31	0.51± 0.08	9.42± 0.70
J00440332+0228112	21	1348± 60	1290± 18	0.46± 0.07	8.49± 0.56
J01073866-1314134	21	1351± 60	1295± 6	0.44± 0.06	8.50± 0.46
J04433761+0002051	21	2157± 30	2500± 637	0.78± 0.97	30.51±23.47
J05361998-1920396	21	1749± 62	1590± 49	0.82± 0.16	12.24± 0.61
J08195820-0335266	21	1038± 38	1014± 21	-0.03± 0.03	6.16± 0.55
J19355595-2846343	21	2386± 3	2885± 343	0.74± 0.79	60.86± 5.54
J20004841-7523070	21	2302± 11	2904± 363	0.87± 0.76	61.27± 5.77
J20135152-2806020	21	2170± 29	2581± 578	0.82± 0.91	38.36±27.34
J20153059-4215419	21	1346± 60	1277± 33	0.53± 0.11	8.45± 0.49
J21171431-2940034	21	1268± 56	1233± 19	0.30± 0.12	8.00± 0.48
J21140802-2251358	21	1212± 53	1176± 12	0.47± 0.08	7.55± 0.44
J22081363+2921215	21	1697± 63	1569± 38	0.67± 0.19	11.74± 0.87
J22443167+2043433	21	1242± 55	1185± 6	0.49± 0.09	7.53± 0.40
J22533287-2539475	21	1470± 64	1372± 19	0.60± 0.18	9.40± 0.63
J225540.75-311842.0	21	760± 23	673± 16	-0.07± 0.12	3.51± 0.25
J232304-015232	21	923± 23	885± 20	-0.09± 0.05	5.13± 0.44
J23542220-0811289	21	1475± 64	1359± 9	0.63± 0.09	9.15± 0.53
CWISE J050626.96+073842	21	1216± 53	1176± 0	0.54± 0.00	7.49± 0.52
J00344300-4102266	36	1794± 60	1696± 41	0.67± 0.10	14.95± 0.86
J05184616-2756457	36	2052± 42	1937± 308	1.09± 0.18	19.17± 1.65
J05361998-1920396	36	1876± 56	1719± 42	0.93± 0.10	15.44± 1.09
J23231347-0244360	36	2288± 13	2712± 297	1.07± 0.15	43.18± 6.17
J00132229-1143006	47	1078± 42	1077± 12	0.03± 0.05	8.46± 0.91
J00205014-1519129	47	1417± 62	1357± 20	0.49± 0.09	11.19± 0.99

Table B.1. Masses of sub-stellar objects with ages in the range 10-200 Myr derived using AMES models (cont...)

Name	Age Myr	T_{eff} (BC) K	T_{eff} (remap) K	r	Mass M_{Jup}
J0045214+163445	47	1888± 55	1777± 68	0.86± 0.11	17.05± 1.62
ULAS J004757.40+154641.4	47	1101± 44	1092± 24	0.17± 0.02	8.62± 1.03
J02074284+0000564	47	851± 10	837± 19	-0.03± 0.04	6.27± 0.82
J02022917+2305141	47	1358± 60	1302± 11	0.46± 0.09	10.68± 1.05
WISE J024124.73-365328.0	47		1289± 1	0.59± 0.26	10.45± 0.91
J00303013-1450333	47	1360± 60	1322± 32	0.35± 0.03	10.73± 1.13
ULAS J075829.83+222526.7	47	809± 0	775± 16	-0.07± 0.06	5.51± 0.74
PSO J168.1800-27.2264	47	1069± 41	1075± 16	0.05± 0.04	8.63± 0.95
ULAS J120744.65+133902.7	47	819± 3	790± 14	-0.08± 0.04	5.88± 0.73
J12574463-3635431	47	2337± 5	2658± 286	0.83± 0.32	40.66± 4.90
J15104786-2818174	47	2411± 7	2732± 206	0.83± 0.31	47.17± 5.06
J15210327+0131426	47	1071± 41	1078± 13	0.05± 0.04	8.61± 0.81
ULAS J154701.84+005320.3	47	880± 16	863± 16	-0.04± 0.05	6.45± 0.81
J21324036+1029494	47	1472± 64	1413± 29	0.50± 0.09	11.85± 1.18
J23512200+3010540	47	1424± 63	1373± 23	0.45± 0.10	11.74± 1.18
J00065794-6436542	37	2365± 1	2784± 270	0.99± 0.33	48.74± 6.43
J00182834-6703130	37	1894± 54	1758± 63	0.87± 0.26	16.11± 1.51
J00191296-6226005	37	1860± 57	1736± 56	0.83± 0.13	15.98± 1.39
J00381489-6403529	37	2001± 47	1941± 79	0.72± 0.33	19.85± 1.86
J01174748-3403258	37	1866± 56	1743± 57	0.83± 0.13	15.82± 1.60
J01205114-5200349	37	1815± 59	1686± 47	0.80± 0.11	14.68± 1.38
J01415823-4633574	37	1938± 52	1817± 195	0.95± 0.20	17.59± 7.06
J01531463-6744181	37	1743± 62	1606± 55	0.80± 0.22	13.79± 1.12
J02103857-3015313	37	1866± 56	1762± 58	0.77± 0.19	16.27± 1.53
J02410564-5511466	37	1827± 58	1703± 53	0.78± 0.16	15.42± 1.18
J03420931-2904317	37	1761± 61	1714± 61	0.45± 0.19	14.74± 1.43
J03421621-6817321	37	1726± 62	1576± 49	0.89± 0.14	13.98± 7.15
J04400972-5126544	37	1848± 57	1713± 62	0.85± 0.17	15.46± 1.45
J21544859-7459134	37	2117± 35	2089± 336	1.04± 0.26	22.88± 5.39
J22134491-2136079	37	1913± 53	1795± 239	0.89± 0.21	16.33± 1.35
J22351658-3844154	37	1860± 57	1759± 63	0.75± 0.20	16.21± 1.49
J22353560-5906306	37	2081± 39	2033± 218	0.91± 0.36	21.88± 1.83
J23225299-6151275	37	1812± 59	1699± 54	0.75± 0.13	15.25± 1.39
CWISE J050626.96+073842	21	1216± 53	1176± 0	0.54± 0.00	7.49± 0.52
J00011217+1535355	137	1660± 64	1712± 20	0.69± 0.04	25.67± 1.71
J00325584-4405058	137	1854± 57	1960± 18	0.97± 0.07	33.68± 1.94
J00425923+1142104	137	2052± 42	2267± 54	1.08± 0.07	47.01± 1.75
WISEP J004701.06+680352	137	1295± 58	1295± 16	0.55± 0.06	16.77± 0.94
J02260907-1609591	137	1344± 60	1342± 26	0.60± 0.03	17.77± 1.17
PSO J039.6352-21.7746	137	1749± 62	1901± 45	0.45± 0.06	31.52± 2.92
J02583123-1520536	137	1833± 58	1890± 34	1.01± 0.06	31.10± 2.81
J03164512-2848521	137	1863± 56	1975± 49	0.91± 0.08	33.82± 1.91
J03264225-2102057	137	1520± 64	1530± 37	0.66± 0.04	21.35± 1.50
J03552337+1133437	137	1520± 64	1507± 25	0.74± 0.04	21.05± 1.82
J04185879-4507413	137	1552± 65	1601± 48	0.54± 0.10	23.55± 1.48
ULAS J081918.58+210310.4	137	913± 21	943± 14	-0.07± 0.04	11.34± 0.71
J10451718-2607249	137	2110± 36	2377± 49	1.09± 0.05	54.34± 4.68
J11101001+0116130	137	932± 24	975± 19	-0.02± 0.02	11.83± 0.92
J13243553+6358281	137	1105± 44	1133± 11	0.26± 0.05	14.30± 0.92
J14252798-3650229	137	1595± 65	1631± 14	0.67± 0.05	23.72± 1.53
WISEPA J062720.07-111428	137	901± 20	939± 11	-0.06± 0.02	11.22± 0.69

Table B.1. Masses of sub-stellar objects with ages in the range 10-200 Myr derived using AMES models (cont...)

Name	Age Myr	T_{eff} (BC) K	T_{eff} (remap) K	r	Mass M_{Jup}
WISE J163645.56-074325.1	137	1041± 38	1091± 23	-0.00± 0.04	13.68± 1.02
WISE J174102.78-464225.5	137	1442± 63	1451± 33	0.57± 0.03	19.44± 1.48
PSO J306.0+16	137	1729± 62	1791± 19	0.76± 0.08	27.98± 1.80
J20490268-7456124	137	1341± 60	1345± 26	0.55± 0.03	17.67± 1.15
PSO J318.4+35	137	1906± 54	2040± 48	1.05± 0.06	36.66± 3.10
J21572060+8340575	137	2068± 40	2238± 52	1.10± 0.00	45.09± 3.38
J22064498-4217208	137	1643± 64	1695± 26	0.73± 0.04	25.52± 1.74
J22443167+2043433	137	1242± 55	1244± 10	0.47± 0.04	15.96± 1.01
J23433470-3646021	137	1674± 64	1661± 37	0.97± 0.07	24.95± 2.13
J23360735-3541489	137	2007± 46	2167± 40	1.10± 0.00	42.38± 2.21
J23433470-3646021	137	1674± 64	1663± 40	0.98± 0.06	25.28± 1.84
PSO J358.5+22	137	1773± 61	1880± 35	0.69± 0.06	31.05± 2.11
PSO J004.6359+56.8370	200	952± 27	1016± 24	-0.01± 0.02	14.66± 2.41
SIMP J013656.5+093347.3	200	1085± 42	1163± 30	0.11± 0.04	17.45± 2.74
J01033203+1935361	200	1325± 59	1366± 35	0.53± 0.07	21.86± 3.81
J04371868-5509449	200	1467± 64	1500± 36	0.70± 0.07	24.81± 4.27
J04590034-2853396	200	1344± 60	1402± 36	0.48± 0.06	22.57± 4.07
J07235265-3309446	200	1674± 64	1735± 54	0.95± 0.10	31.83± 5.89
J11544223-3400390	200	2049± 42	2314± 123	1.10± 0.00	55.11± 11.51
J14413716-0945590	200	1956± 50	2137± 86	1.07± 0.06	45.74± 8.07
J15530228+1532369	200	851± 10	886± 21	-0.10± 0.03	11.86± 1.93
ULAS J130217.21+130851.2	200	761± 47	680± 27	-0.06± 0.15	8.72± 1.43
ULAS J131610.13+031205.5	200	1270± 56	1355± 35	0.24± 0.04	20.92± 3.39
J13262009-2729370	200	1318± 59	1376± 41	0.46± 0.05	22.17± 4.39
J16241436+0029158	200	841± 8	876± 24	-0.06± 0.03	12.18± 1.95
J21392676+0220226	200	1114± 45	1167± 28	0.30± 0.04	17.27± 2.90
J21543454-1055308	200	1506± 64	1555± 33	0.74± 0.07	26.94± 4.23
J22361685+5105487	200	950± 27	1013± 28	0.01± 0.02	14.72± 2.31